Available online at www.sciencedirect.com
ScienceDirect
Engineering Fracture Mechanics 73 (2006) 2723–2747
Engineering Fracture Mechanics
www.elsevier.com/locate/engfracmech

Influence of statistical and constraint loss size effects on cleavage fracture toughness in the transition – A model based analysis

H.J. Rathbun [1], G.R. Odette *, M.Y. He, T. Yamamoto

Materials and Mechanical Engineering Departments, University of California, Santa Barbara, CA 93106, United States

Received 17 November 2005; received in revised form 23 April 2006; accepted 9 May 2006
Available online 27 June 2006

Abstract

A database derived from tests on specimens with a large range of ligament (b) and thickness (B) dimensions was systematically analyzed to evaluate constraint loss and statistical size effects on cleavage fracture toughness. The objectives were to: (1) decouple size effects related to constraint loss, mediated by b and B, from those arising from statistical effects, primarily associated with B; and, (2) develop procedures to transfer toughness data to different conditions of constraint and B. The toughness database for a Shoreham pressure vessel steel plate, tested at a common set of conditions, was described in a companion paper. Quantification of constraint loss was based on an independently calibrated 3D finite-element critical stress-area, $\sigma^* - [K_{J_m}/K_{J_c}]$, model. The measured toughness data, K_{J_m}, were first adjusted using computed $[K_{J_m}/K_{J_c}]$ constraint loss factors to the corresponding values for small scale yielding conditions, $K_{J_c} = K_{J_m}/[K_{J_m}/K_{J_c}]$. The K_{J_c} were then statistically adjusted to a K_{J_r} for a reference $B_r = 25.4$ mm. The B adjustment was based on a critically stressed volume criterion, modified to account for a minimum toughness, K_{min}, consistent with modest modifications of the ASTM E 1921 Standard procedure. The combined $\sigma^* - [K_{J_m}/K_{J_c}] - K_{min}$ adjustment procedure was applied to the Shoreham $b - B$ database, producing a homogeneous population of K_{J_r} data, generally within the expected scatter. The analysis suggests that: (1) there may be a maximum B beyond which statistical size effects diminish, and (2) constraint loss in the three-point bend specimens begins at a relatively low deformation level. A corresponding analysis, based on a Weibull stress, $\sigma_w - [K_{J_m}/K_{J_c}] - K_{min}$, adjustment procedure, yielded similar, but somewhat less satisfactory, results. The optimized adjustment procedure was also applied to other K_{J_m} data for the Shoreham plate from this study, as well as a large database taken from the literature. The population of $489 K_{J_r}$ data points, covering an enormous range of specimen sizes, geometries and test temperatures, was found to be consistent with the same master curve $T_0 = -84$ °C derived from the $b - B$ database. Thus, calibrated micromechanical models can be used to treat size and geometry effects on K_{J_m}, facilitating using small specimens and data transfer to predict the fracture limits of structures.

Keywords: Cleavage toughness; Constraint effects; Statistical effects; Cleavage fracture models; Master curve method

* Corresponding author. Tel.: +1 805 893 3525; fax: +1 805 893 8651.
E-mail address: odette@engineering.ucsb.edu (G.R. Odette).
[1] Currently with University of California, Lawrence Livermore National Laboratory, United States.

0013-7944/$ - see front matter © 2006 Elsevier Ltd. All rights reserved.
doi:10.1016/j.engfracmech.2006.05.009

Nomenclature

A	stressed area
$\langle A \rangle$	stressed area averaged over the crack front thickness direction
A_0	non-dimensional stressed area
A_p	plastic area under the load–displacement curve use to calculate J
A^*	critical area
A_{ssy}	stressed area under small scale yielding conditions
a	crack length
B	specimen thickness
B_{max}	thickness limit for statistical size scaling
B_r	reference thickness
b	ligament size
c_i	linear regression coefficients
C_i	polynomial regression coefficients for the non-dimensional stressed area as a function of σ_{22}/σ_y
d_{eff}	effective trigger particle size
E	elastic modulus
J	elastic–plastic J-integral
J_m	critical measured J_I equivalent to K_{J_m}
J_c	critical J at SSY
J_{cr}	J_c equivalent to K_{J_r} at the reference thickness B_r
J_{crs}	small scale yielding J_{cr} at the reference thickness B_r
J_{crl}	large scale yielding J_{cr} at the reference thickness B_r
J_p	experimental plastic J
K_I	mode I stress intensity factor
K_J	elastic–plastic K derived from J
K_{J_c}	small scale yielding toughness
$K_{J'_c}$	nominal SSY value for a specified B
K_{J_m}	measured K_J at cleavage
$K_{J_{max}}$	maximum value of toughness
K_{J_0}	maximum likelihood median toughness
K_{J_r}	reference K_J
K_{J_B}	K_{J_m} adjusted to thickness B
K_{min}	threshold K below which $P_f = 0$
K_u	K_{J_c} at $P_f = 0.63$
$[K_{J_m}/K_{J_c}]$	computed constraint loss adjustment factor
m_σ	Weibull strength modulus
m_k	Weibull toughness modulus
M	in-plane deformation factor $\equiv b\sigma_0/J = E\sigma_0 b/K^2_{J_m}$
M_{lim}	data censoring limit with $M_{lim} = 30$ in ASTM E 1921 procedure
n	fit for B_{max}
n_s	number of SSY toughness data points
n_l	number of LSY toughness data points
p	B-size scaling exponent
P_f	fracture probability
R	σ_{22}/σ_y
S	loading span for bend tests
T	temperature
T_0	reference temperature
V^*	critical stressed volume

V_r	reference volume
W	specimen width
x, y	spatial dimensions in vicinity of crack tip
z	out-of-plane, thickness direction position
δ	CTOD
ε	strain
ϕ_{ssy}	square root of the sum of the squares of J_{crs}
ϕ_{lsy}	square root of the sum of the squares of J_{crl}
σ	stress
σ^*	critical stress
σ_y	yield stress
σ_w	Weibull stress
σ_u	Weibull stress at $P_f = 0.63$
σ_1	first principal stress
σ_{22}	normal stress tensor component in the y-direction perpendicular to the crack plane
σ_{min}	minimum Weibull stress
η	factor to define J_p from A_p as $J_p = \eta A_p/bB$
v	Poison's ratio
$\rho(m_\sigma)$	error metric for the difference between ϕ_{ssy} and ϕ_{lsy}
$\langle x \rangle$	average value of variable x

Acronyms

3PB	single edge notched 3 point bend specimens
AP	adjustment procedure
ASTM	American Society for Testing and Materials
CDF	cumulative distribution function
CT	compact tension specimen
CL	constraint loss
FE	finite element
LSY	large scale yielding
PCC	pre-cracked Charpy
PPC	post processing code
SSY	small scale yielding
SPCC	shallow pre-cracked Charpy
UCSB	University of California Santa Barbara

1. Introduction and background

It is well known that measured values of fracture toughness often depend on the test specimen size and geometry. For example, materials science textbooks typically describe the increase in toughness associated with the transition from conditions of plane strain to plane stress with decreasing specimen thickness (B – see Fig. 1 showing standard specimen geometries). However, this is only one manifestation of size effects that are related to the stress and stress-state distributions in the local volume of material near the tip of a blunting crack. Under plane strain, the crack tip stresses are higher than the materials' flow stress due to triaxial constraint, with peak stresses $\geqslant 3$ times the yield stress, σ_y. In general, the crack tip stress fields depend on the true stress–strain constitutive properties of the material, $\sigma(\varepsilon)$, the size and geometry of the cracked body and loading. Loading is described by the elastic–plastic J, or equivalent $K_J = \sqrt{[J(1-v^2)/E]}$, where E and v are the elastic modulus and Poisson's ratio, respectively. For limited conditions of deep cracks with $a/W \approx 0.5$, (where a is the crack depth, W the specimen width and S the loading span – see Fig. 1) loaded in bending, and with a small plastic zone embedded in a larger elastic region, the stress fields have a self-similar, fixed shape in distances normalized

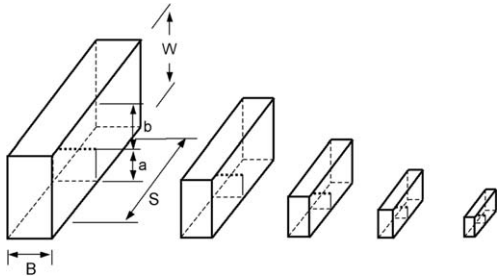

Fig. 1. Standard 3PB specimens of various sizes with self-similar geometry.

by $J/[b\sigma_y]$, or the crack tip opening displacement, δ. Such small scale yielding (SSY) fields depend on the constitutive properties and J, but are independent of the size and geometry of the cracked body.

Size and geometry factors that reduce the amplitude of the crack tip stress fields below SSY levels are responsible for what are collectively known as constraint loss effects. There is a large literature on constraint loss effects based on finite element simulations of crack tip fields for various specimen configurations.[2] Constraint loss increases measured fracture toughness, K_{J_m}, of body-centered cubic alloys in the cleavage transition over corresponding SSY values, K_{J_c}, $(K_{J_m}/K_{J_c} > 1)$.[3] Even under plane strain conditions, constraint loss is caused by large scale in-plane plastic deformation, when the size of the plastic zone is no longer small compared to the uncracked ligament, b, or other key cracked body dimensions, leading to a size dependence of K_{J_m}. For example, non-singular compressive T-stress fields, associated with shallow cracks or loading in tension, reduce constraint and increase K_{J_m} [1–3].

In addition to constraint loss effects, there are also statistical size effects related to the volume of material under high stress near the crack tip. At equal SSY J-loading, the highly stressed volume increases roughly with the specimen thickness, B (neglecting side-surface effects). A larger volume increases the statistical probability that a sufficiently high stress will encounter a sufficiently weak, so-called, trigger particle that produces a propagating microcrack resulting in macroscopic cleavage. Trigger particles include large grain boundary carbides, or clusters of carbides, and other brittle inclusions. The trigger particles fracture under the high crack tip stress fields, enhanced by local strain incompatibilities. However, the critical event is continued propagation of the particle nucleated cleavage microcrack through the ferrite matrix. Based on a modified Griffith criterion, the stress required to produce a propagating microcrack varies as $1/\sqrt{d_{\text{eff}}}$, where d_{eff} is the effective trigger particle size. The probability of triggering a large weak microcrack nucleation site not only varies with the stressed volume, but also from specimen to specimen. Thus, statistical effects are also responsible for the natural scatter in measured cleavage fracture toughness.

The American Society for Testing and Materials (ASTM) standard E 1921, "*Standard Test Method for Determination of Reference Temperature, T_0, for Ferritic Steels in the Transition Range*" specifically recognizes both constraint loss and statistical size effects [4]. Constraint loss effects are treated indirectly, by a censoring procedure, that assumes a maximum value of toughness, $K_{J_{max}} = (E'\sigma_y b/30)^{1/2}$, when a test K_{J_m} exceeds a plastic deformation limit defined by a parameter M

$$M = \frac{E'\sigma_y b}{K_{J_m}^2} < 30 \tag{1}$$

where $E' = E/(1-\nu^2)$. The censored data are combined with uncensored $K_{J_m} < K_{J_{max}}$, and then statistically adjusted to a reference thickness, $B_r = 25.4$ mm, based on an equivalent stressed volume resulting in an equal probability of fracture, P_f, that is 0 below a minimum K_{min}, as,

[2] The literature on constraint loss effects is far too extensive to fully cite. Pertinent information can be found in Anderson [2], scientific papers in ASTM STP proceedings on Fracture, Fatigue and Fracture and two conferences specifically focused on constraint loss effects, proceedings of various ASME PVP symposia, as well in archival journals such as Engineering Fracture Mechanics and International Journal of Fracture. Hence, here we will cite only the most pertinent and representative references.

[3] The crack tip stress state also influences ductile fracture toughness associated with the nucleation, growth and coalescence of microvoids. However, we focus here on the effects of specimen size and geometry on cleavage initiation fracture toughness.

$$K_{J_B} = [K_{J_m} - K_{min}]\left[\frac{B}{B_r}\right]^{1/4} + K_{min} \quad (2)$$

Analysis of a large database used to establish the master curve method in ASTM E 1921 resulted in a best fit value of $K_{min} = 20$ MPa $\sqrt{m}$ [4,5]. The K_{J_B} are then used to evaluate a maximum likelihood median toughness, K_{J_0}, as well as the corresponding temperature T_0 at $K_{J_0} = 100$ MPa $\sqrt{m}$, based on the assumption of a universal master toughness temperature curve shape. The master curve method also allows setting lower and upper bound confidence limits on cleavage toughness–temperature curves. More detailed discussion of the implications of our study to the ASTM E 1921 Standard are presented elsewhere [6]. Here, we focus on distinguishing between the two mechanisms that lead to size (and geometry) effects by quantitatively modeling their consequences to K_{J_m}. The calibrated model can then be used to adjust K_{J_m} data to SSY K_{J_c} values and the K_{J_c} to a reference toughness, K_{J_r}, at the reference B_r.

Before proceeding further, it is useful to summarize and explain the logical nomenclature used in this paper.

- K_{J_m} is the measured toughness that may depend on both constraint loss and statistical size effects.
- K_{J_c} is the K_{J_m} adjusted to SSY conditions at a specified B, that may be lower than K_{J_m} due to constraint loss effects.
- K_{J_B} is the statistically adjusted K_{J_m} at B_r, that may be higher or lower than K_{J_m} due to statistical effects.
- K_{J_r} is the SSY toughness at B_r.
- K_{J_0} is the median toughness (note that ASTM E 1921 uses $K_{J_{c(med)}}$ to define median toughness).

This non-standard nomenclature supports the basic objective of this work, which is to quantify the differences between K_{J_m} and K_{J_c} due to constraint loss effects and K_{J_c} and K_{J_r} due to statistical effects.

Prior to developing the database described in the companion paper [7], there was no direct basis to unambiguously discriminate constraint loss from statistical size effects. This was due to the fact that the vast majority of toughness data was for specimens that varied in dimension, but had self-similar geometries, like the ones shown in Fig. 1, with a relatively small range of B/b ratios. Notably, models of the initial stages of constraint loss predict roughly the same size scaling as statistical size effects ($b^{-1/4}$ versus $B^{-1/4}$) in self-similar specimens [8]. Thus, reductions in B attributed to statistical size effects could actually be associated with reductions in b originating from constraint loss effects.

The statistical size effect adjustment has a reasonable physical foundation based on the fact that, for SSY, the highly stressed volume scales as BK_J^4. Thus, equal stressed volumes for two different B (B_1 and B_2) require a corresponding applied K_J ratio, $K_{J_1}/K_{J_2} = [B_2/B_1]^{1/4}$. This volume scaling does not itself provide a basis for a K_{min}, which is theoretically based on conditional probability concepts [2]. Indeed, it is not clear that K_{min} is a constant, or if it depends on other factors, such as K_{J_0}, or varies with temperature and/or from material to material.

Alternative micromechanical models based on sympathetic events along the crack front [9], or process zone damage coalescence instabilities [10] leading to cleavage could be expected to modify a simple and unbounded $[B_2/B_1]^{1/4} - K_{min}$ type scaling. Further, both upper and lower B limits on $[B_2/B_1]^{1/4} - K_{min}$ type scaling can be anticipated for a variety of reasons. Physical limits on the trigger particle distribution would be expected to place some absolute upper bound on B for such scaling. It has also been proposed that B-scaling cannot reduce K_{J_c} below the equivalent arrest toughness value [11]. Further, an isolated microscopic pop-in damage event, that would be sub-critical at larger B, may occupy a significant area fraction of the ligament in very thin specimens, leading to immediate macroscopic fracture.

In order to better distinguish between constraint loss and statistical size effects, a full matrix of three point bend fatigue pre-cracked fracture specimens with B from 8 to 254 mm (6 sizes) and b from 3.2 to 25.4 mm (4 sizes) were fabricated from a single plate of steel taken from the Shoreham reactor pressure vessel and tested at −91 °C at an otherwise common set of conditions. The experimental details and $b - B$ database developed in this single variable study are described in a companion paper [7]. We focus here on an analysis of this $b - B$ database using both deterministic and statistical micromechanical models coupled with three-dimensional (3D) finite element (FE) simulations of the crack tip stress fields. The deterministic model was calibrated to the local fracture properties of the Shoreham steel based on an independent set of fracture tests. The statistical

model was self-calibrated, using the overall $b - B$ database. The single variable database combined with the model-based analysis has allowed, for the first time, an explicit de-coupling of statistical and constraint loss mediated size effects. Further, the calibrated adjustment procedure facilitates both the use of small specimens, and the transfer of such test data to predicting the fracture limits of structures.

The deterministic model was based on a critical stress, σ^*-critical stressed volume, V^*, criterion modified by a $K_{\min}$. The necessary calibration of σ^* was based on a set of high constraint data independent of the $b - B$ matrix. The procedure adjusts the measured K_{J_m} data to the SSY K_{J_c} using a calculated $[K_{J_m}/K_{J_c}]$ constraint loss factor, as $K_{J_c} = K_{J_m}/[K_{J_m}/K_{J_c}]$, and then adjusts K_{J_c} to K_{J_r} with a modified statistical size effect scaling of the general type given in Eq. (2), but with various modifications described below. The model based $[K_{J_m}/K_{J_c}]$ is based on FE calculations that specify the conditions when loading to K_{J_c} under SSY and K_{J_m} in an actual test, at deformation levels beyond SSY, or large scale yielding (LSY), result in the same thickness averaged in-plane stressed area, $\langle A(\sigma_{22})\rangle$, within a contour for a specified stress normal to the crack plane, $\sigma_{22} = \sigma^*$. For a given B, the cleavage fracture condition is that $\langle A(\sigma^*)\rangle = A^*$. The subsequent use of the statistical size effect adjustment with a modified form of Eq. (2) then establishes conditions for equal stressed volumes, modified by a probability of cleavage fracture $P_f = 0$ below $K_{\min}$, as well as a possible saturating effect of B. Note, the sequential application of the constraint loss and statistical size effect adjustments is necessary to use the $K_{\min}$ modification for equivalent stressed volumes as represented by Eq. (2). These combined steps are referred to as the $\sigma^* - [K_{J_m}/K_{J_c}] - K_{\min}$ adjustment procedure (AP).

A second adjustment procedure was based on the Weibull stress, σ_w, concept. Here, the statistical probability, P_f, for fracture is a function of an applied Weibull stress, σ_w, loading parameter, a minimum stress, $\sigma_{\min}$, below which the probability of fracture is 0 and two other material parameters that are found by fits to the $K_{J_m} b - B$ database. The Weibull stress exponent, m_σ, is the best-fit exponential weighting of the crack tip stress distribution in computing σ_w, and σ_u is the σ_w at $P_f = 0.63$. The Weibull model was self-calibrated by defining $b - B$ database groups that represent SSY conditions and various subsets of the $b - B$ database that represent LSY conditions, or a mix of LSY and SSY. The $\sigma_w - J$ trajectory up to the point of fracture was evaluated for both SSY conditions and the specific specimen geometry. The ratio of the critical specimen J_m at fracture to the corresponding SSY J (J_c) at the same σ_w was used to establish the corresponding $[K_{J_m}/K_{J_c}]$. The K_{J_c} were then adjusted to K_{J_r}, again using various modifications to Eq. (2). The self-calibration involves finding an optimal m_σ that results in a minimum difference between the root mean square of the SSY and adjusted K_{J_r} $b - B$ datasets, plus additional criteria described below. We refer to this approach as the $\sigma_w - [K_{J_m}/K_{J_c}] - K_{\min}$ AP. Note, since the $\sigma_w - [K_{J_m}/K_{J_c}]$ adjustments intrinsically involve a stressed volume and $\sigma_{\min}$, it might be assumed that the Weibull model does not require a separate B-scaling adjustment. However, the use of $\sigma_{\min}$ does not have the same effect as $K_{\min}$. Overall, the $\sigma_w - [K_{J_m}/K_{J_c}] - K_{\min}$ adjustments were generally less satisfactory than those for the $\sigma^* - [K_{J_m}/K_{J_c}] - K_{\min}$ AP.

The paper proceeds as follows. Section 2 describes the $\sigma^* - [K_{J_m}/K_{J_c}] - K_{\min}$ AP, and the resulting de-coupling and quantification of statistical versus constraint loss effects on K_{J_r}. Section 3 presents the corresponding $\sigma_w - [K_{J_m}/K_{J_c}] - K_{\min}$ AP, and compares its predictions to those of the $\sigma^* - [K_{J_m}/K_{J_c}] - K_{\min}$ AP. Section 4 applies the $\sigma^* - [K_{J_m}/K_{J_c}] - K_{\min}$ AP to the $b - B$ database and additional UCSB data, including some independent low constraint K_{J_m}, as well as to a database of the Shoreham steel, from tests using conventional specimens over a wide range of temperatures, reported by Joyce and Tregoning. The results of this study are summarized in Section 5.

2. The $\sigma^* - [K_{J_c}/K_{J_m}] - K_{\min}$ model

2.1. Finite element simulations of crack tip stress fields

The $\sigma^* - [K_{J_m}/K_{J_c}]$ constraint loss adjustment factor was computed by finite element (FE) simulations of the crack tip stress fields using the general purpose ABAQUS FE code [12] based on the small strain approximation. The material property input to the FE simulations are the elastic modulus E(=207.9 GPa), Poison's ratio ν(=0.29), σ_y and true plastic stress–strain constitutive law, $\sigma(\varepsilon)$, for the Shoreham steel. The $\sigma(\varepsilon)$ was measured using tensile tests over a range of temperatures, including at the test condition for the $b - B$ matrix at −91 °C. The crack tip stress in the y-direction normal to the $x - z$ crack plane, σ_{22}, was used to define cleav-

age conditions; note, σ_{22} is similar to the first principal stress. The area, $A(\sigma_{22}/\sigma_y)$, within a normalized σ_{22}/σ_y stress contour was evaluated as a function of the non-dimensional $J/[b\sigma_y]$. Following Nevalainen and Dodds [13], the SSY $A_{ssy}(K_J,\sigma_{22}/\sigma_y)$ were computed based on a plane strain elastic boundary layer analysis. The SSY boundary layer mesh consisted of 1200 two-dimensional, eight-noded plane strain elements. The finite radius mesh was very refined near the crack tip, and increased in size out to a large boundary radius to ensure that the plastic zone was deeply embedded in an elastic zone. Elastic displacements were imposed on the boundary nodes with a T-stress equal to 0. As expected, the $A(\sigma_{22})$ increased in proportion to K_J^4. The post-processing procedures are described below.

A quarter-symmetry mesh composed of 2480 20-noded quadratic brick elements was used in the 3D FE simulations of $A(K_J,\sigma_{22}/\sigma_y,z)$ for all the independent specimen geometries in the $b-B$ matrix, where z is the out of plane, thickness direction position. In addition to the crack tip fields for the $b-B$ matrix at -91 °C, FE simulations were also carried out for both smooth sided and side-grooved compact tension specimens, as well as deep and shallow pre-cracked bend specimens with $B/W=0.5$ and 1 over a range of temperatures corresponding to all the other test data analyzed in this study. Wedge-shaped elements, with overlapping nodes at an initially sharp crack tip, were used to model blunting up to high levels of plastic deformation, corresponding to a minimum M of less than 10. The out of plane direction was divided into 10 mesh layers that decreased in thickness from the specimen middle to the surface at a constant ratio of 0.8, in order to better account for the out-of-plane z-direction stress field and J gradients. Bend tests were simulated by applying specified increments of displacement to the loading pin in the middle of the specimen spanning two support pins. The path independence of J computed by ABAQUS was verified and sensitivity studies were carried out to assure the adequacy of the baseline mesh. Note, the σ_{22} fields based on the small strain approximation (dictated by the size of the 3D FE calculations) continue to increase above the corresponding peak for an analogous large geometry change, large strain blunting solutions. However, except in some very special circumstances described below, the small strain approximation had little or no effect on the results or conclusions of this study.

A post-processing code (PPC) was developed to determine the $A_{ssy}(\sigma_{22}/\sigma_y)$ and $A(\sigma_{22}/\sigma_y)$. The PPC reads in all nodal coordinates, stress and J-integral values for each deformation increment in the ABAQUS simulation. The PPC then determined the nodes surrounding a specified σ_{22}/σ_y stress contour point on designated radial lines emanating from the crack tip, as shown in Fig. 2. The coordinate on this line at the specified σ_{22}/σ_y was obtained by linear interpolation between the stresses and positions of the bounding nodes. The total area within the stress contour was then calculated as a sum of the corresponding areas of the individual radial segments. The thickness-averaged J and corresponding average stressed areas $\langle A(\sigma_{22}/\sigma_y, K_J)\rangle$ were based on the

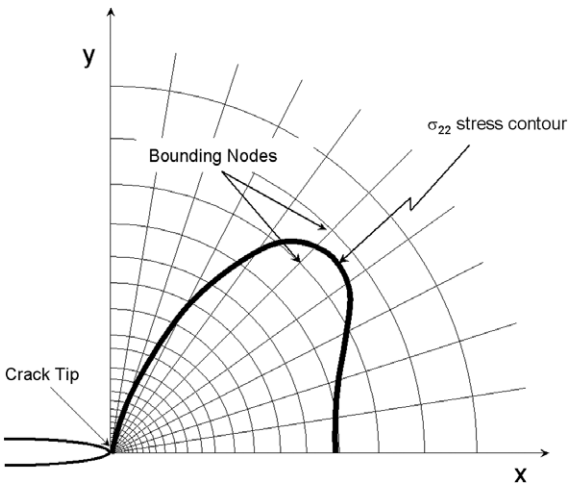

Fig. 2. Illustration of the evaluation of the in-plane area, A, within a stress σ_{22}/σ_y stress contour.

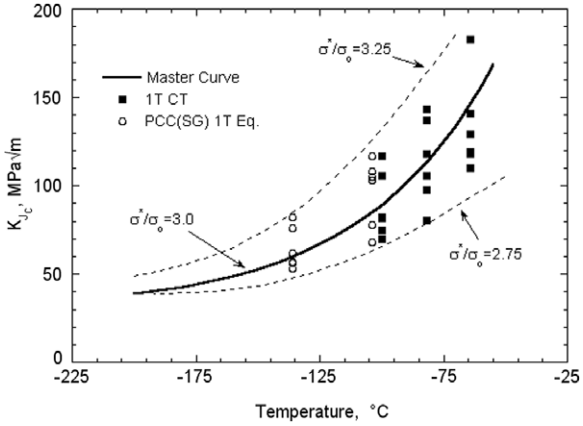

Fig. 3. The $\sigma^* - A^*$ model fit to the high constraint characterization data.

volume-weighted average of the 10 out-of-plane sections. The load–displacement results were also used along with the average J to compute η-factors[4] for the various non-dimensional specimen geometries.

Both the SSY and 3D FE methods used in this study were verified by comparisons to the results of Nevalainen and Dodds [13] and other workers [15]. Note, however, that since some of the details of the 3D versus 2D plane strain SSY FE computations and analysis procedures were slightly different, the nominal $[K_{J_m}/K_{J_c}]$ falls slightly below unity at high M (e.g., $M \gtrapprox 200$ for $\sigma_{22}/\sigma_y \approx 3$). Thus, no constraint adjustment is applied for specimens with measured $M \geqslant 200$ or $[K_{J_m}/K_{J_c}] < 1$. Note that one reason for $[K_{J_m}/K_{J_c}] < 1$ in some cases for large M values is due to the large positive T-stress in deep noded specimens. Finally, since A_{ssy} scales with K_J^4 it is not necessary to evaluate directly K_{J_m} and K_{J_c} at a common $A_{ssy} = \langle A \rangle$ since, in practice, it is simpler to use the equivalent $[K_{J_m}/K_{J_c}] = [A_{ssy}(K_J)/\langle A(K_J)\rangle]^{1/4}$ relation. However, it was necessary to calibrate the model for σ^* for the Shoreham steel.

2.2. Calibration of $\sigma^* - [K_{J_m}/K_{J_c}]$ CL factor adjustment procedure

For a given constitutive law [E, ν and $\sigma(\varepsilon)$] and specimen geometry, $[K_{J_m}/K_{J_c}]$ is a function of K_J and $\sigma_{22}/\sigma_y = \sigma^*/\sigma_y = R$. In deeply cracked bend specimens, $[K_{J_c}/K_{J_m}]$ increases with decreasing R, or lower σ_{22}, due to increased distance from the crack tip. Thus, to apply the σ^*-model we must estimate σ^* for the Shoreham plate. This was done using a $\sigma^* - A^*$ model for $K_{J_c}(T)$, where T is temperature, developed to predict the shape of the SSY master curve [14]. The model uses an empirical $\sigma_y(T)$ and assumes that σ^* and A^* are constant and independent of temperature below $\approx$0 °C. For SSY conditions, $A_{ssy}(\sigma_{22}, K_J)$ increases with K_J^4, and cleavage occurs when at $A_{ssy}(\sigma^*, K_{J_c}) = A^*$. The finite element A_{ssy} results can be represented in a compact non-dimensional form, A_0, as [13]

$$A_0 = \log\left[A_{ssy}(\sigma_{22}/\sigma_y)\sigma_y^4/K_J^4\right] \tag{3}$$

The FE evaluation of the SSY $A_0(\sigma_{22}/\sigma_y)$ was fitted (C_0, C_1, C_2) to a simple polynomial as

$$A_0(\sigma_{22}/\sigma_y) = C_0 + C_1(\sigma_{22}/\sigma_y) + C_2(\sigma_{22}/\sigma_y)^2 \tag{4}$$

Eqs. (3) and (4) can be used to evaluate K_{J_c} at specified values of $\sigma_{22} = \sigma^*$, $A_{ssy} = A^*$ as

$$K_{J_c}(T) \approx \sigma_y(T)[A^* 10 A_0(\sigma^*/\sigma_y)]^{1/4} \tag{5}$$

Eq. (5) can be calibrated by fitting the set of SSY $K_{J_c}(T)$ data shown in Fig. 3. The independent set of calibration data, statistically adjusted to a thickness of 25.4 mm, and assumed to represent SSY conditions, was used

[4] The η factor is use to define the experimental plastic $J(J_p)$ from the plastic area under the load displacement curve (A_p) as $J_p = \eta\, A_p/bB$.

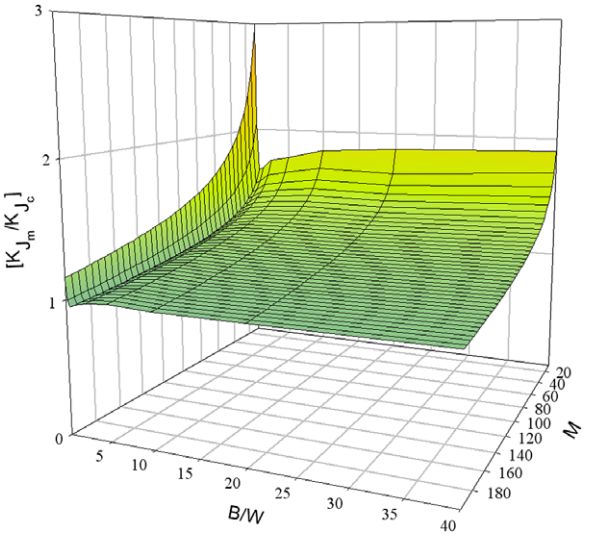

Fig. 4. The computed $[K_{J_m}/K_{J_c}]$ factor for $R = 3$ versus M and B/W.

to estimate $\sigma^* - A^*$ for the Shoreham plate. The filled squares are data from 25.4 mm thick compact tension specimens (1TCT) and the open circles are 10 mm thick pre-cracked Charpy specimens (PCC). In both cases, the specimens were pre-cracked with $a/W \approx 0.5$ and side grooved to a depth of $0.1B$ on each side. The data are adjusted to a common $B_r = 25.4$ mm. Assessment of the preliminary data gave a master curve $T_0 \approx -91$ °C. This T_0 and the data are consistent with the predictions of Eq. (5) shown as the solid line for $A^* = 3.7 \times 10^{-8}$ m^2 and $\sigma^*/\sigma_y = 3.0$. Note, the additional fitting criterion for A^* was that the predicted $K_{J_c}(T)$ be consistent with the master curve shape in the lower shelf-knee regime with a minimum K_{J_r} of ≈30 MPa $\sqrt{\text{m}}$. The dashed lines for $\sigma^*/\sigma_y = 2.75$ and 3.25 bound the data. The calibration data set was re-examined with the final constraint loss adjustment model to verify that it provided a good SSY basis for calibration of σ^*.

Fig. 4 shows the predicted $[K_J/K_{J_m}]$ versus $M = b\sigma_y E'/K_J^2$ for $R = 3$ and various B/W at −91 °C. Constraint loss is rapid and large for small $B/b \leqslant 0.6$. This can be understood in terms of rapid loss of out-of-plane constraint (or conditions that approach plane stress for much of the specimen thickness). The results also suggest that slightly higher constraint loss occurs at larger $B/b \geqslant 5$. This may due to the fact that, in bending, these specimens act more like cracked plates than cracked beams. Note that anticlastic deformations may play a role at large B/W; however, both FE analysis and strain gauging measurements suggested that they had a minimum effect on the test results themselves [15].

2.3. Statistical size adjustments

In the companion paper, we showed that the $b - B$ database is generally consistent with statistical size adjustments given in Eq. (2). In this study, we consider combinations of three modifications of the basic ASTM E 1921 model: (1) a B-scaling exponent p that is not fixed at 0.25; (2) a K_{min} that is not fixed a 20 MPa $\sqrt{\text{m}}$; (3) a maximum B limit, B_{max}, on statistical scaling. Thus, a generalized form of Eq. (2) used for fitting the average adjusted K_{J_c} data at the various B, $\langle K_{J_c}(B)\rangle$

$$\langle K_{J_c}(B)\rangle = [\langle K_{J_c}(B_r)\rangle - K_{min}]\left[\frac{B_r}{B'}\right]^{1/4} + K_{min} \tag{6a}$$

$$B' = B_{max}[1 - \exp(-B/B_{max})^n]^{1/n} \tag{6b}$$

Here, $\langle K_{J_c}(B_r)\rangle$, p, K_{min} and B_{max} are the fitting parameters. A value of $n = 10$ that provides rapid transition to a saturating B limit for statistical scaling was used in this study. The value of $n = 10$ was used for numerical convenience, but itself bears no physical significance, other than that the B-effect saturates above some size for

the test matrix in this study. Since there is a strong covariance between p and K_{min}, only one of these parameters could be fit at a time, while the other must be set at a fixed value.

2.4. Application of the $[K_{J_m}/K_{J_c}] - K_{min}$ constraint adjustment procedure

Fits of Eq. (6) to the averaged $[K_{J_m}/K_{J_c}]$ adjusted $\langle K_{J_c}(B)\rangle$ data were carried out for four variations of the statistical adjustment procedure: (1) $p = 0.25$, $K_{min} = 20$ MPa $\sqrt{m}$ and no B_{max} (the ASTM E 1921 procedure); (2) $p = 0.25$ and $K_{min} = 20$ with a fitted B_{max}; (3) $K_{min} = 20$ MPa $\sqrt{m}$ with fitted p and B_{max}; and (4) $p = 0.25$, with fitted K_{min} and B_{max}. The fit results are shown in Fig. 5 and summarized in Table 1. Fig. 6 shows the corresponding average $\langle K_{J_t}\rangle$ for all $b - B$ combinations as a function of B. Linear regression statistical tests of the significance of the c_1 and c_2 coefficients of least square fit expressions in the form of $\langle K_{J_t}\rangle = c_1 + c_2 B$ show no significant overall systematic trend with B, except for the ASTM model without a B_{max}, with $\langle K_{J_t}\rangle = 86.9 + 0.0555B$. This suggests that there may be a maximum limit for statistical B-scaling

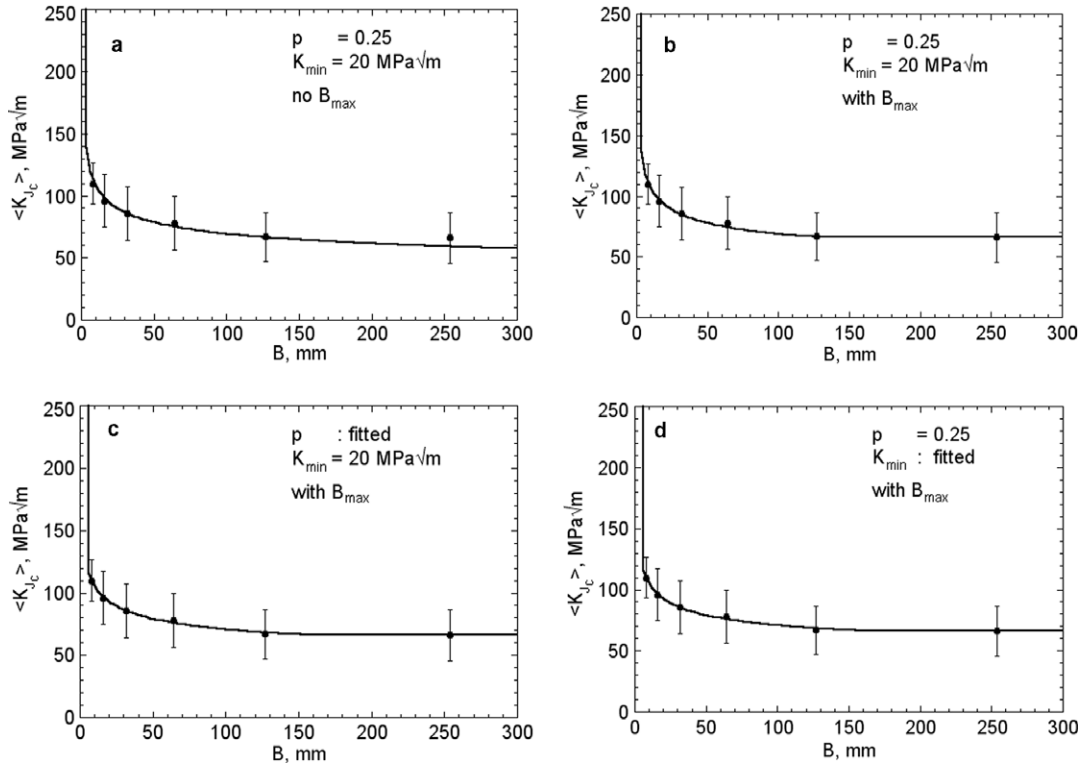

Fig. 5. The $\langle K_{J_c}(B)\rangle$ versus B for the $\sigma^* - [K_{J_m}/K_{J_c}] - K_{min}$ AP for the four B-scaling models.

Table 1
Fit parameters for the four different B-scaling models

B-scaling model	K_{J_t} (MPa $\sqrt{m}$)	p	K_{min} (MPa $\sqrt{m}$)	B_{max} (mm)	SD[a] (MPa $\sqrt{m}$)
ASTM E 1921	89.7 ± 1.7	0.25	20	–	10.2
ASTM w/B_{max}	88.8 ± 0.98	0.25	20	121.6 ± 20.7	8.7
p fitted w/B_{max}	89.3 ± 0.66	0.224 ± 0.01	20	153.6 ± 24.8	8.5
K_{min} fitted w/B_{max}	89.1 ± 0.67	0.25	26.8 ± 2.7	157.3 ± 29.5	8.7

[a] Standard deviation of the adjusted $\langle K_{J_t}(b,B)\rangle$ data.

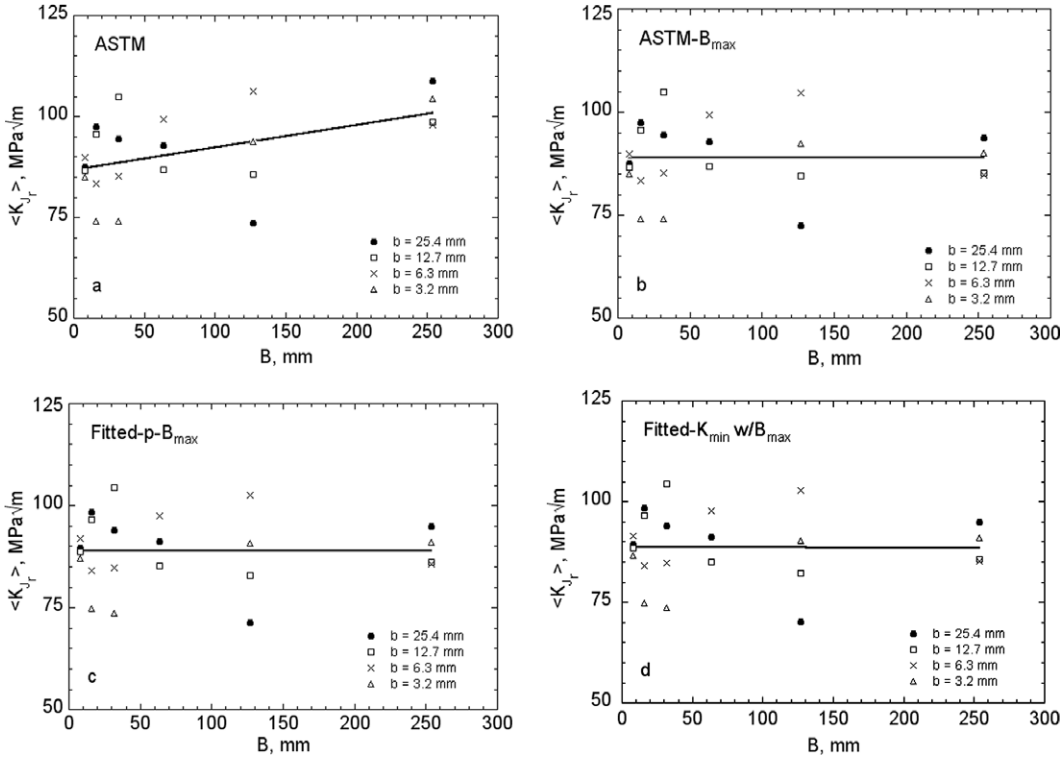

Fig. 6. The $\langle K_{J_r}(B,b)\rangle$ versus B for the $\sigma^* - [K_{J_m}/K_{J_c}] - K_{min}$ AP for the four B-scaling models.

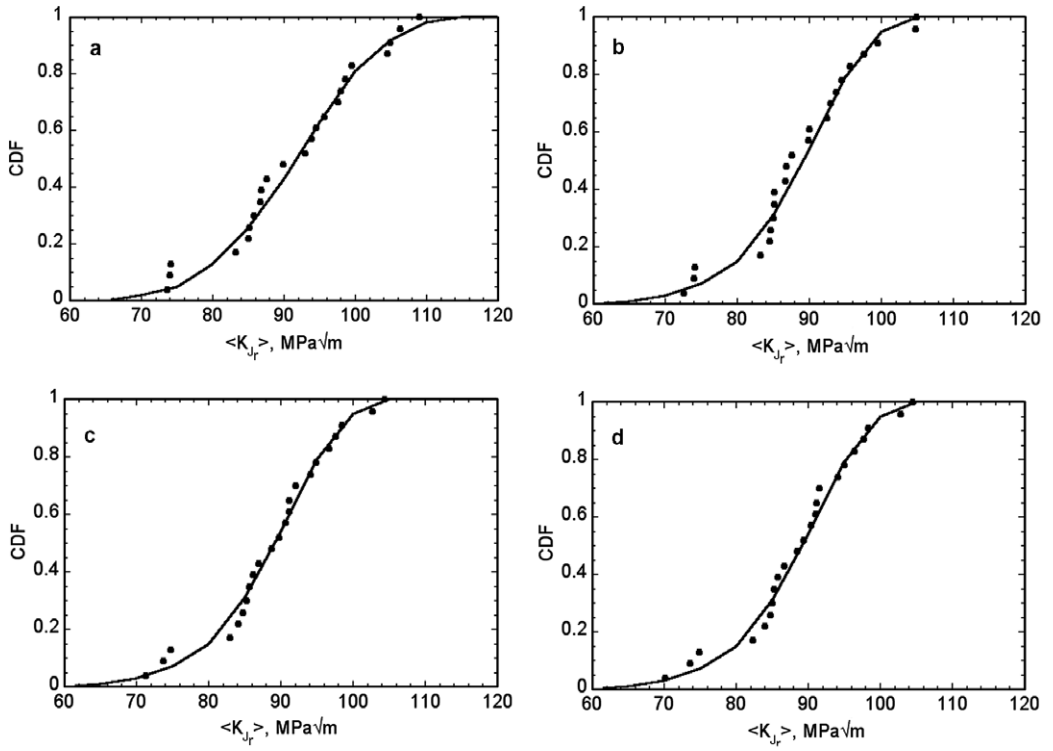

Fig. 7. The CDF of all the averaged $\langle K_{J_r}\rangle$ data for the $\sigma^* - [K_{J_m}/K_{J_c}] - K_{min}$ AP for the four B-scaling models.

in the $b - B$ database, with a $B_{max} \approx 120$–160 mm. This conclusion is also consistent with an analysis of only high constraint data with $[K_{J_m}/K_{J_c}] \leqslant 1.05$, which reduces possible bias introduced by the constraint adjustments.

Similar fits to $\langle K_{J_r} \rangle = c_3 + c_4 b$ showed no significant and systematic effect of b, although on average $\langle K_{J_r} \rangle$ for the smallest $b = 3.2$ mm is somewhat lower than for the others (see discussion below). This is primarily associated with low average values of K_{J_m}, hence, $\langle K_{J_r} \rangle$ for $b = 3.2$ mm at both $B = 16$ and 32 mm. However,

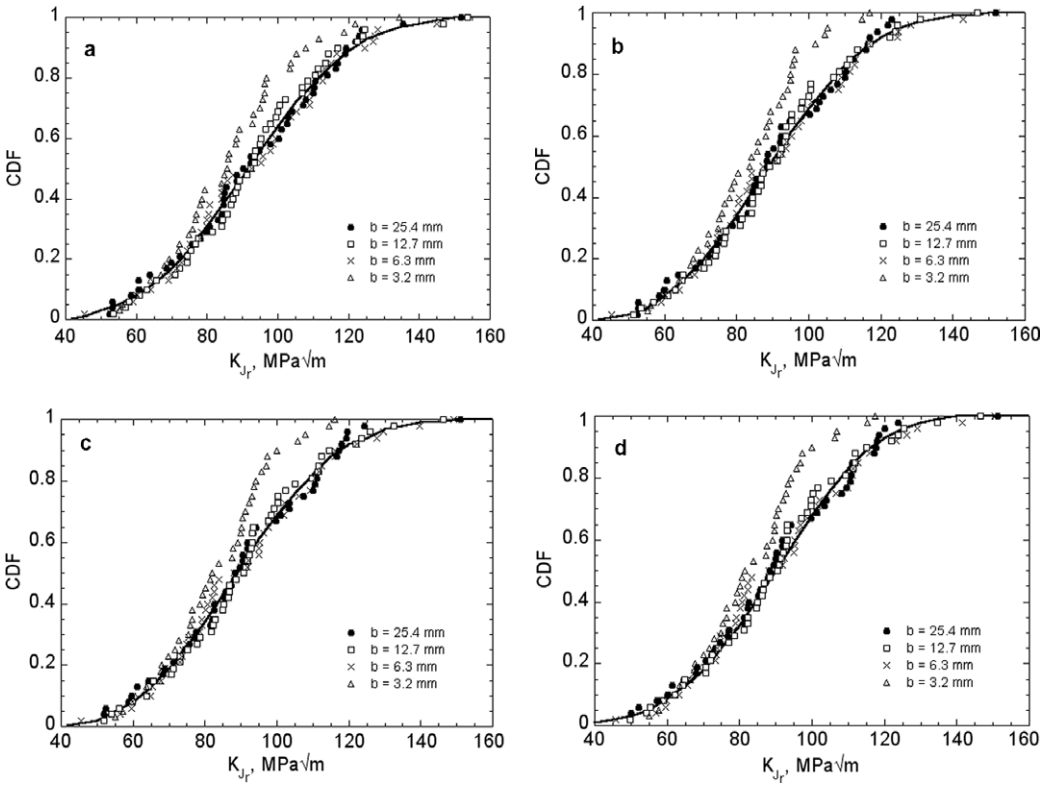

Fig. 8. The CDF of all the K_{J_r} data for the $\sigma^* - [K_{J_m}/K_{J_c}] - K_{min}$ AP for the four B-scaling models.

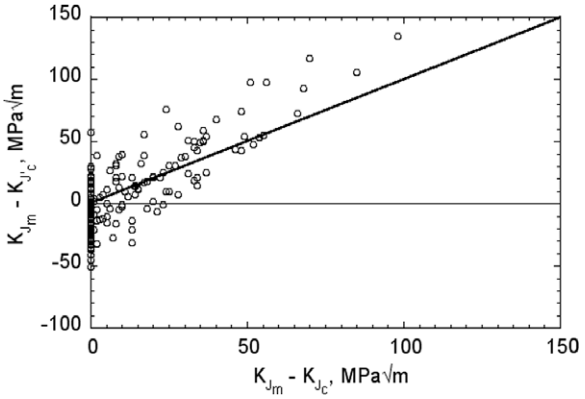

Fig. 9. An empirical estimate of the constraint loss, $(K_{J_m} - K_{J'_c})$, versus the $\sigma^* - [K_{J_m}/K_{J_c}] - K_{min}$ AP, $(K_{J_m} - K_{J_c})$, for the fitted p and B_{max} statistical-scaling model.

there is also a $\langle K_{J_r} \rangle$ point for $b = 25.4$ mm and $B = 127$ mm that is even lower. The scatter in the $\langle K_{J_r} \rangle$ of ≈8.5–10.2 MPa $\sqrt{m}$ is consistent with both standard statistical estimates and Monte Carlo simulations predict standard deviation of the average $\langle K_{J_r} \rangle$ for 8 tests per $b - B$ condition of ≈8.2 MPa $\sqrt{m}$ for an overall population of K_{J_r} data with a standard deviation of about ≈±23 MPa $\sqrt{m}$.

Fig. 7 shows the corresponding cumulative distribution function (CDF) plots of the $\langle K_{J_r} \rangle$ data along with a fitted normal distribution function. Fig. 8 shows CDF plots and fits to all the $b - B$ K_{J_r} data (184 points) for the various b. In all cases, the smallest $b = 3.2$ mm specimens have lower adjusted toughness values, especially at $K_{J_r} \geqslant$ ≈98 MPa $\sqrt{m}$; below this value the smaller deviations are <7 MPa $\sqrt{m}$ lower than the average CDF for the specimens with the three larger b values. The overall standard deviation of the K_{J_r} data is also lower for the $b = 3.2$ mm dataset.

These differences might be attributed to over-adjustment of the K_{J_m} data by the $\sigma^* - [K_{J_m}/K_{J_c}] - K_{min}$ procedure, since the $b = 3.2$ mm specimens generally suffer the larger constraint loss. The difference between the overall CDF for the $b = 3.2$ mm and other data with larger b is greater for all the models with a B_{max}. This is because most (5/7) of the $b = 3.2$ mm data at $K_{J_r} \geqslant 98$ MPa $\sqrt{m}$ are for specimens with the largest $B = 127$ and 254 mm (note this number is 11/15 for $K_{J_r} \geqslant 90$ MPa $\sqrt{m}$). Both the higher K_{min} (for $p = 0.25$) and lower p (for $K_{min} = 20$ MPa $\sqrt{m}$) models with a B_{max} result in a smaller (for $B = 127$ mm) to a much smaller (for $B = 254$ mm) statistical B-scaling adjustment ($K_J/K_{J_c} > 1$) compared to the ASTM E 1921 model (no B_{max} and fixed $p = 0.25$ and $K_{min} = 20$ MPa $\sqrt{m}$). Thus, in addition to possible small over-adjustments for constraint loss, these deviations in the higher part of the K_{J_r} CDF distribution for the $b = 3.2$ mm specimens could be due to experimental bias, especially in cases with large B and hence very atypical B/b ratios of about 40–80.

The potential for bias in the $b = 3.2$ mm specimens can be qualitatively understood in terms of the sensitivity of K_{J_m} to b and a/W. The K_{J_m} were based on the nominal a/W for each specimen evaluated using a standard 9 point averaging procedure, with an overall average of 3.0 ± 0.33 mm for all the specimens. However, variations in a/W across the crack front were not accounted for in evaluating the K_{J_m}. Of course, the effects of such a/W deviations is greatest for $b = 3.3$ mm specimens. Further, the a/W deviations are expected to be generally more pronounced for larger B. Since cleavage would tend to initiate at the largest a/W, the data would be biased towards lower K_{J_m}, due to a potentially higher actual applied K_I stress intensity factor at the site of fracture than given by the nominal a/W. Further, it is conceivable that, due to alloy heterogeneities, the fatigue pre-crack depth tends to be largest in the most brittle regions along a crack front, where initiation is also most likely to occur. Differences in T-stresses and non-linear elastic–plastic loading would amplify a crack depth bias effect. Thus, the deviations in CDF for $b = 3.2$ mm specimens may be partly due to experimental bias in the data.

We have not carried out a more detailed evaluation that attempts to correlate the local initiation site and crack depth in each case, nor have we fully quantified the effects of crack front depth deviations on a potential bias in the K_{J_m} data. However, examination of the 9-point average database used to establish the nominal a/W for all the specimens supports the hypothesis outlined above. The deepest crack front deviations are largest for the $b = 3.2$ mm specimens, averaging 5.7%, versus 1.5% for the larger b cases. Further, the deepest a/W deviate from the average ≈5–18% (averaging ≈10%) in the $b = 3.2$ specimens with $B \geqslant 127$ mm, compared to 1–7% (averaging ≈3%) for the thinner specimens with $B \leqslant 32$ mm. Notably, corresponding deviations for the shallowest crack fronts are much smaller.

Another approach to assessing the potential for constraint loss over-adjustment is to inversely adjust the overall population average $\langle K_{J_r} \rangle = 91.3$ MPa $\sqrt{m}$ to the corresponding nominal SSY value for a specified B, $K_{J'_c}(B)$, using a selected B-scaling model. Assuming the B-scaling model is correct, the resulting $K_{J_m}(B) - K_{J'_c}(B)$ provide an empirical estimate of constraint loss, albeit one that is scattered due to the intrinsic statistical distribution of the actual K_{J_m} data itself. Fig. 9 plots $K_{J_m} - K_{J'_c}$ versus the $\sigma^* - [K_{J_m}/K_{J_c}] - K_{min}$ constraint loss adjustment, $K_{J_m} - K_{J_c}$, for the fitted p and B_{max} statistical-scaling model. As expected, the data is scattered, but the general trend shows that $K_{J_m} - K_{J'_c}$ is actually greater than $K_{J_m} - K_{J_c}$, especially for larger adjustments. This is directly opposite to the trend that would be expected if the $\sigma^* - [K_{J_m}/K_{J_c}]$ procedure over adjusts the K_{J_c} data.

In order to further distinguish the four models, Weibull plots were constructed by assigning a CDF lowest to highest K_{J_r} ranked probability of fracture, P_f, given by

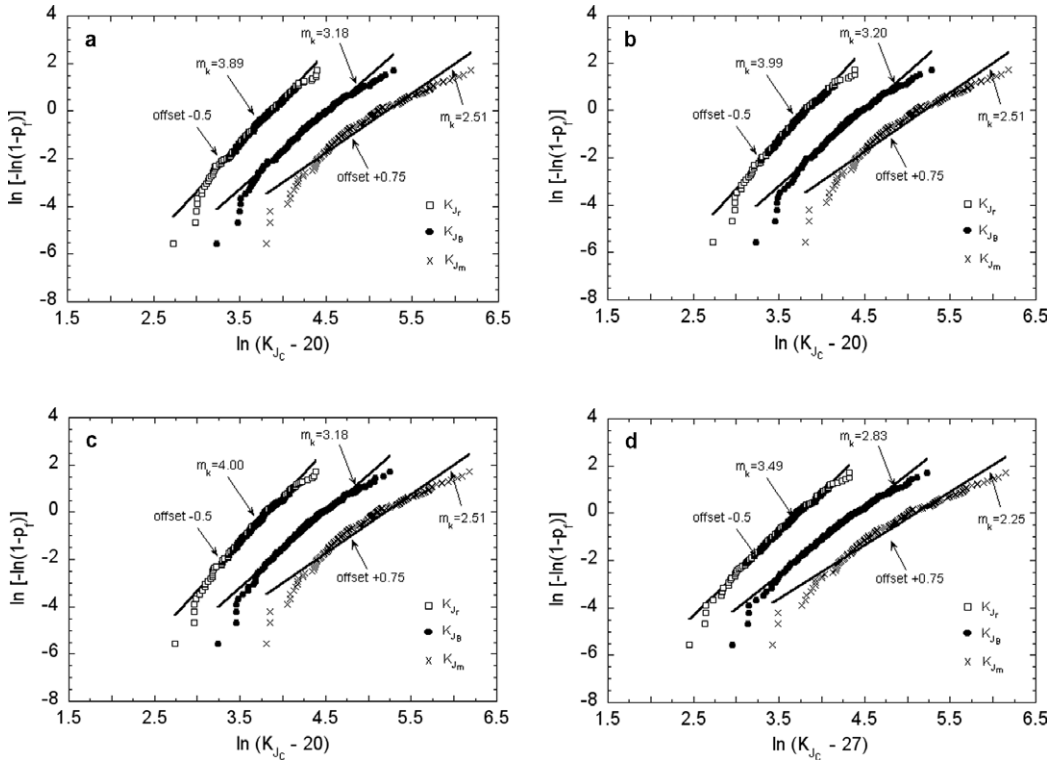

Fig. 10. Weibull plots of K_{J_m}, K_{J_B} and K_{J_r} for the $\sigma^* - [K_{J_m}/K_{J_c}] - K_{\min}$ AP for the four B-scaling models.

$$P_f = 0 \quad K_J < K_{\min} \tag{7a}$$

$$P_f = 1 - \exp\left\{-\left[\frac{K_{J_r} - K_{\min}}{K_u - K_{\min}}\right]^{m_k}\right\} \quad K_J > K_{\min} \tag{7b}$$

Here, $K_u = K_{J_c}$ at $P_f = 0.63$. For a critically stressed volume model, modified by $K_{\min}$, $m_k = 4$, or $1/p$. More generally, plots of $\ln[-\ln(1 - P_f)]$ versus $\ln[K_J - K_{\min}]$ have a slope of m_k and an ordinate equal to 0 at $P_f = 0.63$. Fig. 10 shows the Weibull plots, including the measured toughness K_{J_m} (offset by +0.75); the measured toughness adjusted for statistical B-scaling, K_{J_B}; and K_{J_r} (offset by −0.5) for the four statistical B-scaling models. Assuming P_f in the form given by Eq. (7), the deviations from the least squares fit lines at high tough-

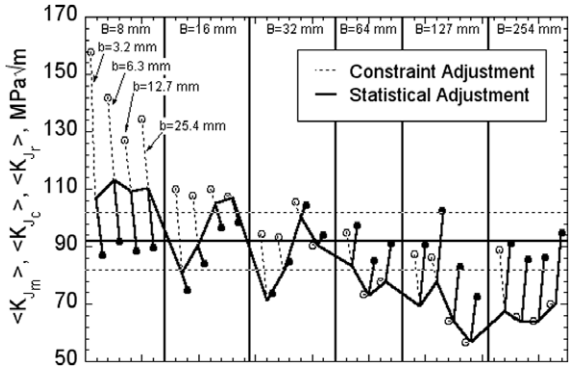

Fig. 11. The $\langle K_{J_m}\rangle$, $\langle K_{J_c}\rangle$ and $\langle K_{J_r}\rangle$ adjustments as a function of b and B showing the pattern of constraint loss and statistical adjustments.

ness indicate loss of constraint. Deviations at low toughness indicate that Eq. (7) does not describe well the lower tail of the toughness distribution.

The combined constraint loss and statistical adjustments provide reasonable K_{J_r} Weibull distributions with minimum deviations from a best-fit m_k. The least squares fits show that all the models with $K_{\min} = 20$ MPa $\sqrt{\text{m}}$ give a m_k close to the nominal value of 4. For the fitted $K_{\min} = 26.8$ MPa $\sqrt{\text{m}}$ model, m_k is lower by ≈3.5. Among the variants, the fitted p and ASTM models with a $B_{\max}$ give a slightly better overall Weibull fit than the others. Again, given the strong covariance, similar fits are provided by other paired combinations of p (≈0.22–0.25) and $K_{\min}$ (≈20–27 MPa $\sqrt{\text{m}}$). For further discussion, we will use the $p = 0.224$, $K_{\min} = 20$ MPa $\sqrt{\text{m}}$ and $B_{\max} \approx 154$ mm model, which appears to give the best overall results.

Fig. 11 shows the pattern constraint loss and statistical adjustments as a function of b and B. The open symbols are measured K_{J_m} data and the filled symbols fully adjusted K_{J_r} data. The dashed line shows the constraint loss adjustment and the solid line the statistical adjustment. The former are dominant at small and intermediate B, while the latter are most important at the larger B. The horizontal dashed lines mark the one standard deviation scatter in $\langle K_{J_r} \rangle$. The strong decrease in $\langle K_{J_m} \rangle$ with increasing B is evident, but it is clear that this is partly due to constraint loss effects. For example, the thinnest specimens with $B \approx 8$ mm suffer significant constraint loss even for the largest ligament with $b = 25.4$ mm. On the other hand, the constraint loss is generally much less for specimens with the largest B, even for $b = 3.2$, due to the fact that the K_{J_m} start out

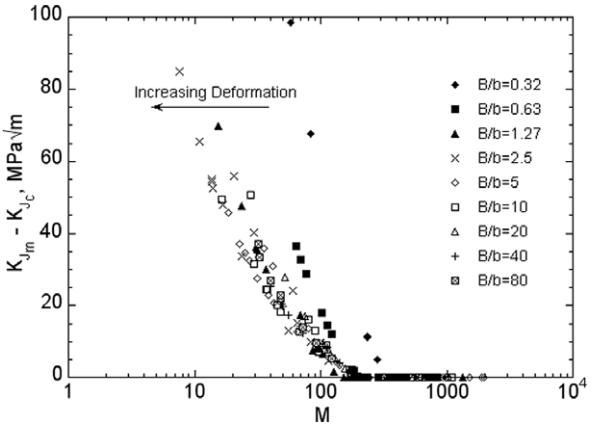

Fig. 12. The magnitude of the constraint adjustments versus M for the various B/b for the $\sigma^* - [K_{J_m}/K_{J_c}] - K_{\min}$ AP.

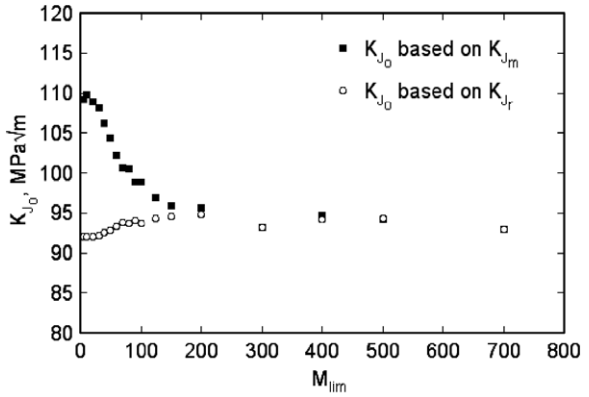

Fig. 13. The K_{J_0} obtained from ASTM E 1921-97 procedure with varied M-limit (M_{lim}) for the measured K_{J_m}, and the $\sigma^* - [K_{J_m}/K_{J_c}] - K_{\min}$ adjusted K_{J_r} toughness data sets.

lower due to the statistical size effects. That is, there is a strong *interaction* between constraint loss and statistical size effects in the $b - B$ matrix, and both must be properly treated in order to understand how they act to influence the measured K_{J_m}.

Fig. 12 shows the magnitude of the calculated constraint loss adjustment, $K_{J_m} - K_{J_c}$, as a function of M for the various B/b. The trends are similar, but the specimens with the smallest $B/b < 1$ lose constraint very rapidly, while the others form a band showing constraint loss beginning at $M \approx 200$. Clearly, constraint loss begins at a deformation level that is much lower than the $M = 30$ censoring limit in the ASTM E921 standard. The implication of this result are discussed elsewhere [6].

Fig. 13 shows the median K_{J_0} for specimens with $B/b > 0.6$ based on the measured K_{J_m} analyzed using the basic ASTM E 1921 procedure, but plotted against a varying limiting value of M ($M_{\lim}$) for data censoring. The K_{J_0} increases systematically below a $M_{\lim}$ starting at about 200. Fig. 13 also shows the corresponding analysis using the fully adjusted K_{J_r} data for the fitted $p - B_{\max}$ statistical adjustment. Clearly, the $\sigma^* - [K_{J_m}/K_{J_c}] - K_{\min}$ AP effectively eliminates the $M_{\lim}$ dependence of K_{J_0}, yielding a value of 100 ± 2 MPa $\sqrt{\text{m}}$. Note, the other statistical adjustment models produce generally similar results.

Thus, in summary, the $\sigma^* - [K_{J_m}/K_{J_c}] - K_{\min}$ AP is effective in producing a homogeneous population of size-adjusted K_{J_r} data. The statistical B-scaling model judged to be best was based on the fitted $p = 0.224$ and $B_{\max} \approx 154$ mm. Note, since the B intervals vary by a factor of 2, this is only an order of magnitude estimate, suggesting that $B_{\max}$ occurs somewhat above 125 mm but significantly below 250 mm. Deviations of some of the $b = 3.2$ mm data from the overall CDF data may, or may not, indicate the possibility of some over adjustment for constraint loss using the $\sigma^* - [K_{J_m}/K_{J_c}] - K_{\min}$ AP. However, this trend has other explanations and a large over-adjustment is not supported by the overall data analysis. If there is some over-adjustment for large values of $[K_{J_m}/K_{J_c}]$ (or $K_{J_m} - K_{J_c}$) it is believed to be modest, and in most cases less than $\approx$10 MPa $\sqrt{\text{m}}$.

3. Weibull stress model

3.1. Overview

There are several important differences between the critical stress-volume, $\sigma^* - [K_{J_m}/K_{J_c}] - K_{\min}$ AP and the statistical Weibull stress, $\sigma_w - [K_{J_m}/K_{J_c}] - K_{\min}$ AP:

- The statistical Weibull stress $\sigma_w - [K_{J_m}/K_{J_c}] - K_{\min}$ AP accounts for the volume averaged power-weighted contribution of high stresses near the crack tip in terms of a loading parameter called the Weibull stress σ_w. In contrast, the $\sigma^* - [K_{J_m}/K_{J_c}] - K_{\min}$ AP treats all stresses equally within a given stress contour.
- The $\sigma_w - [K_{J_m}/K_{J_c}] - K_{\min}$ AP is explicitly based on the probability of fracture, P_f, as a function of the σ_w and local material fracture properties including the Weibull stress modulus, m_σ, and the $\sigma_w = \sigma_u$ at $P_f = 0.63$. The version of the σ_w model used in this study also assumes a minimum threshold Weibull stress $\sigma_{\min}$, below which $P_f = 0$. The $\sigma_{\min}$ is somewhat akin to, and is derived from, $K_{\min}$, but is not functionally equivalent to $K_{\min}$.
- The $\sigma_w - [K_{J_m}/K_{J_c}] - K_{\min}$ AP explicitly depends on the highly stressed volume and manifests an inherent pure $(B/B_r)^{1/4}$-type scaling modified for out of plane constraint loss effects. Hence, the effects of a $K_{\min} > 0$ must be treated using a variant of Eq. (6), and incorporated in the self-calibration fitting procedure.
- The $\sigma_w - [K_{J_m}/K_{J_c}] - K_{\min}$ AP was self-calibrated using the $b - B$ database instead of an independent data set. The calibration involved finding a optimized and self-consistent value m_σ along with a best fit B-scaling model.

As discussed previously, σ_w represents a single loading parameter that accounts for the entire highly stressed volume within the process zone based on a weakest link assumption of the cleavage initiation mechanism [16]. The three-parameter (m_σ, σ_u and $\sigma_{\min}$) σ_w model gives the probability of cleavage fracture P_f as

$$P_f = 1 - \exp\left\{-\left[\frac{\sigma_w - \sigma_{\min}}{\sigma_u - \sigma_{\min}}\right]^{m_\sigma}\right\} \tag{7a}$$

The σ_w is defined as

$$\sigma_w = \left\{ \frac{1}{V_r} \int_{\sigma_1 > 2\sigma_y} \langle \sigma_1 \rangle^{m_\sigma} \, dV(\sigma_1) \right\}^{1/m_\sigma} \tag{7b}$$

Here, $\langle \sigma_1 \rangle$ is the average stress in a mesh element, dV is the corresponding differential volume and V_r is an arbitrary reference volume. The first principal stress, σ_1, was used in evaluating σ_w, rather than the σ_{22} normal stress used in the $\sigma^* - [K_{J_m}/K_{J_c}] - K_{min}$ AP, although the differences between them are small.

A second post-processing code was developed to evaluate σ_w as a function of the elastic–plastic J. The $\langle \sigma_1 \rangle$ for the individual volume elements dV were defined by the finite element mesh as the average of the σ_1 stresses at the 8 corner nodes for the 3D models, and 4 corner nodes for the 2D model. The $\langle \sigma_i \rangle^{m\sigma} \Delta V_i$ for all mesh elements were summed over a process zone region, defined by $\sigma_1 \geqslant 2\sigma_y$ [17,18]. The σ_1/σ_y was truncated at 4.2 since the small strain FE calculations are not accurate very close to the crack tip. The $\sigma_w - J$ trajectory was calculated using 3D FE simulations for each independent specimen geometry in the $b - B$ test matrix, as well as the boundary layer plane strain SSY model. Fig. 14 shows representative σ_w trajectories for both a specimen and SSY model at the same thickness, B. Thus, the measured LSY K_{J_m} to SSY K_{J_c} AP shown in Fig. 14 is similar to the $[K_{J_m}/K_{J_c}]$ common stressed area (A) adjustment, but with the cleavage criteria based on a common σ_w.

The σ_w balances effects of magnitudes of σ_1 with the stress weighted volume under the overall σ_1 distribution. The stressed volume increases with decreasing σ_1. Thus, cleavage may occur for larger volumes under a lower σ_1, or smaller volumes for higher σ_1, where m_σ is the key local material property dictating this balance. The σ_1/σ_y also inversely maps onto the distance from the crack tip. Thus, as m_σ increases, σ_w weights the high, near tip σ_1 stresses more heavily. For a typical m_σ value of order 15, the largest contribution to the σ_w comes from the region between $\sigma_1/\sigma_y \approx 2.6$–$2.8$.

The volume integrated Weibull model itself represents a pure $B^{-1/4}$ scaling. Thus, it is again necessary to separately adjust the K_{J_c} to K_{J_r} to account for a $K_{min} > 0$. This was carried out using the different variants of Eq. (6), as described in the following section on model calibration.

3.2. Calibration and application of the Weibull stress model

Calibration of the Weibull stress (σ_w) model requires determining the m_σ that provides uniform maximum likelihood statistical properties for the entire adjusted K_{J_r} database. Our approach was based on modification of the procedure proposed by Gao and co-workers [17,18]. The $\sigma_w - J$ trajectories were calculated for m_σ between 10 and 20 for all independent specimen geometries in the $b - B$ test matrix, as well as for the plane strain SSY boundary element model to provide a $\sigma_w - [K_{J_m}/K_{J_c}]$ constraint adjustment factor. The remaining statistical sampling effect of B is subsequently addressed by adjusting all toughness values to the reference $B_r = 25.4$ mm using different variants of Eq. (6).

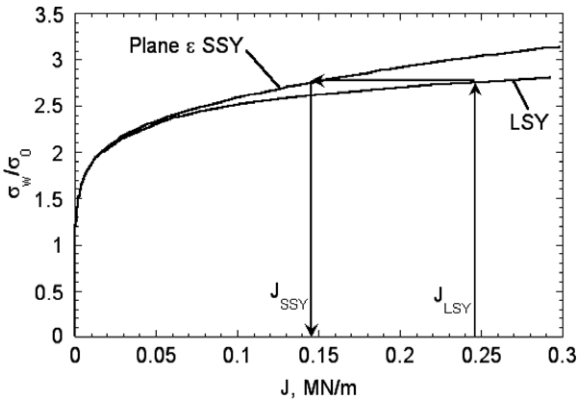

Fig. 14. Illustration of normalized σ_w/σ_y SSY and LSY versus J stress trajectories and the $\sigma_w - [K_{J_m}/K_{J_c}]$ constraint loss adjustment procedure.

The self-calibration involves grouping K_{J_r} data into LSY and SSY subsets. This is justified by the wide range of constraint conditions encountered in the $b - B$ database itself. m_σ can be found by optimizing the overlap between SSY and adjusted LSY data subsets. Note, adjustment of K_{J_m} to K_{J_r} does not require fits to the other Weibull parameters, σ_u and σ_{min}. This fitting was carried out as a separate exercise.

The calibration procedure seeks to minimize the difference between the defined SSY and LSY K_{J_r} datasets using a maximum likelihood statistical parameter ϕ. However, instead of K_{J_r}, the equivalent J_{cr} (J_{crs} and J_{crl} for SSY and LSY, respectively) were used in the minimization. For a specified m_σ,

$$\phi_{ssy} = \frac{1}{n_s}\left[\sum_{i=1}^{n_s} J_{crs_i}^2\right]^{1/2} \tag{8a}$$

$$\phi_{lsy} = \frac{1}{n_l}\left[\sum_{i=1}^{n_l} J_{crl_i}^2\right]^{1/2} \tag{8b}$$

Here, n_s and n_l are the number of adjusted toughness values in the SSY and LSY subsets, respectively. The error metric is given by

$$\rho(m_\sigma) = \frac{\phi_{lsy} - \phi_{ssy}}{\phi_{ssy}} \tag{9}$$

Thus, ρ is less than 0 for over-adjustments of the LSY data and vice versa. The 'best fit' m_σ is defined $\rho(m_\sigma) = 0$, or at the absolute minimum of $\rho(m_\sigma)$ in some cases.

The optimized m_σ depends on both the choice of the B-scaling model (the variant of Eq. (6)) and the choice for the SSY versus LSY division. Various approaches to this division were examined, resulting in different numbers of data points in the two groupings. For example, one simple approach was to determine the SSY

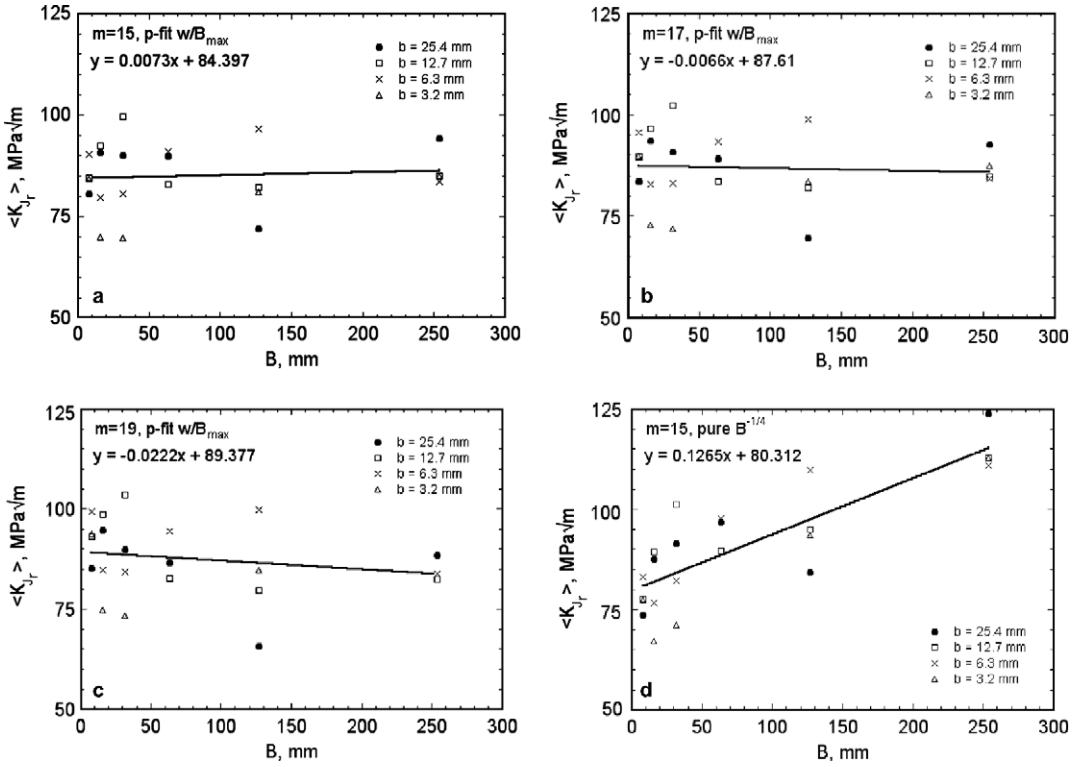

Fig. 15. $\langle K_{J_r}\rangle$ versus B for the $\sigma_w - [K_{J_m}/K_{J_c}] - K_{min}$ AP for a p and B_{max} fitted B-scaling model and: (a) $m_\sigma = 15$, (b) $m_\sigma = 17$ and (c) $m_\sigma = 19$ along with (d) pure Wiebull model $B^{-1/4}$ scaling model with $m_\sigma = 15$.

group based on a maximum constraint loss adjustment specified as 2 MPa $\sqrt{\text{m}}$. However, a disadvantage of this procedure is that the SSY versus LSY split depends on m_σ, and n_s can be small. Another approach was to specify the SSY data subset based on independent definitions of high constraint data, such as $M \geqslant 200$ and $B/b > 1$. A third approach was to use the M_{lim} analysis to set a nominal J_{crs}, and thus ϕ_{ssy}, while evaluating ϕ_{lsy} for various subsets of the measured data. Finally, the J_{crs} were evaluated from $\sigma^* - [K_{J_m}/K_{J_c}] - K_{\min}$ adjusted K_{J_r} data. The different B-scaling approaches were discussed previously in conjunction with the $\sigma_w - [K_{J_m}/K_{J_c}] - K_{\min}$ model.

The alternative SSY versus LSY data partitioning and statistical B-scaling models yield different optimized values of m_σ ranging from ≈12 to 20. The constraint loss adjustments, and corresponding K_{J_r} distributions, depend on m_σ. Further, note that optimizing m_σ does not itself result in a corresponding minimization of size (b, B) effects in the overall K_{J_r} dataset. However, overall minimization of such size effects should be a consideration in selecting between various models.

Analysis of the results of many different models led to the following observations:

- Pure $B^{-1/4}$-scaling, $K_{\min} = 0$ models performed very poorly, irrespective of the LSY–SSY data partitioning procedure, and resulted in both over-adjustments for constraint loss compared to the $\sigma^* - [K_{J_m}/K_{J_c}] - K_{\min}$ procedure, as well as a statistically significant effect of B variations in the adjusted K_{J_r} data. These models also resulted in large deviations in CDF for data from specimens with the smallest $b = 3.2$ mm, with lower values at essentially all toughness levels.
- All models using LSY–SSY partitioning based on the $M - B/b$ limit or the specified constraint loss criteria yielded optimized $m_\sigma \leqslant 15$. Such m_σ values resulted in larger constraint loss adjustments, and more significant deviations in CDF for data from specimens with the smallest $b = 3.2$ mm, compared to the optimized $\sigma^* - [K_{J_m}/K_{J_c}] - K_{\min}$ AP. The deviation increased with decreasing m_σ.
- The ASTM E 1921 procedure did not fully remove the deviation in the K_{J_r} data at the largest B.

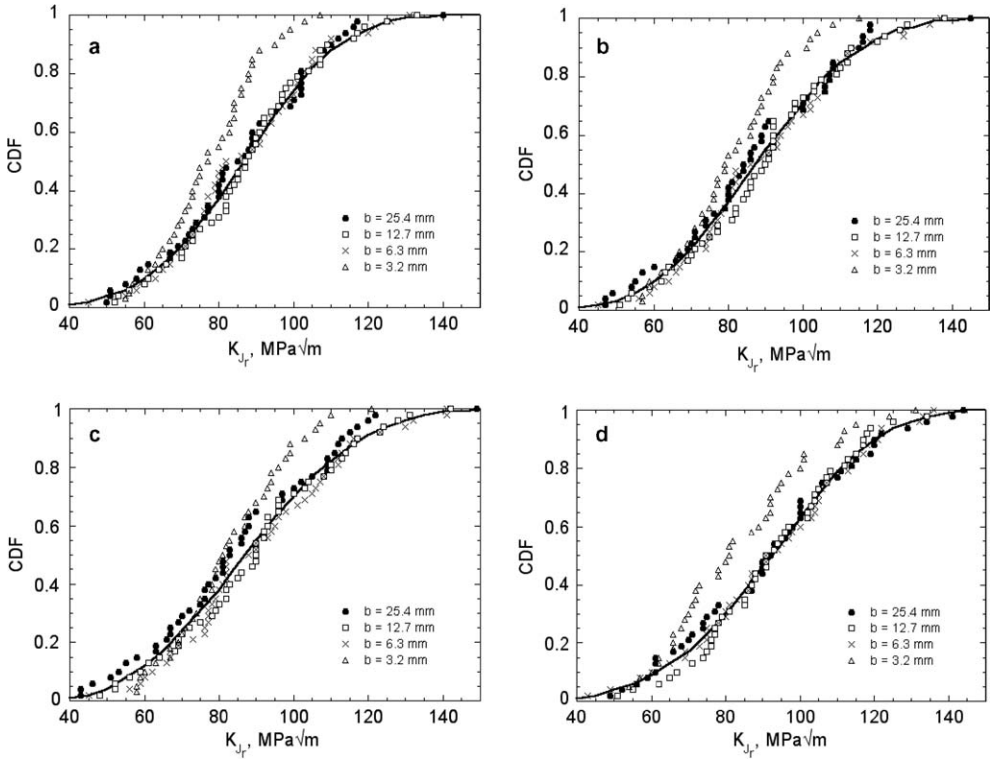

Fig. 16. The CDF for the K_{J_r} data from $\sigma_w - [K_{J_m}/K_{J_c}] - K_{\min}$ AP with p and $B_{\max}$ fitted B-scaling model and: (a) $m_\sigma = 15$, (b) $m_\sigma = 17$ and (c) $m_\sigma = 19$ along with (d) pure Weibull model $B^{-1/4}$-scaling model with $m_\sigma = 15$.

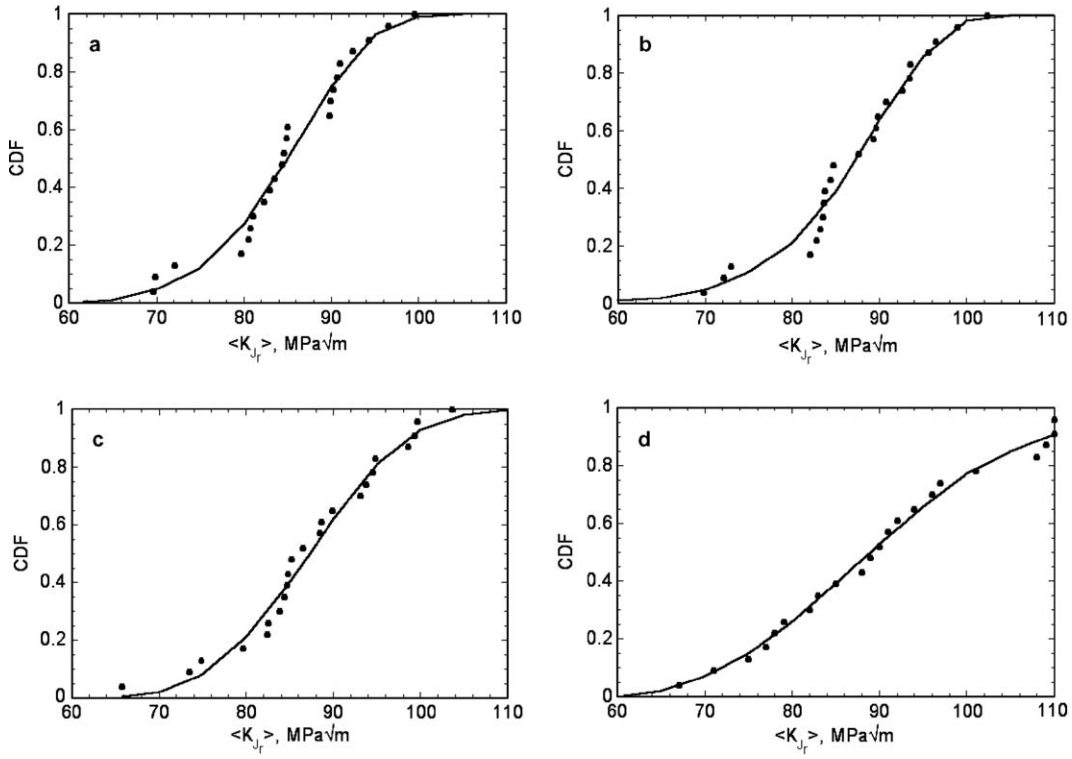

Fig. 17. The CDF for the geometry averaged $\langle K_{J_r} \rangle$ data from $\sigma_w - [K_{J_m}/K_{J_c}] - K_{min}$ AP with p and B_{max} fitted B-scaling model and: (a) $m_\sigma = 15$, (b) $m_\sigma = 17$ and (c) $m_\sigma = 19$ along with (d) pure Wiebull model $B^{-1/4}$ scaling model with $m_\sigma = 15$.

Unfortunately, there is no unique and obviously correct calibration procedure. Thus, we present the results of 3 models with optimized $m_\sigma = 15$ (the ASTM E 1921 and $M \geqslant 200$ and $B/b \geqslant 1$), $m_\sigma = 17$ (B_{max} and p fits and J_{crs} from the M_{lim} analysis) and $m_\sigma = 19$ (B_{max} and p fits and J_{crs} from the $\sigma^* - [K_{J_m}/K_{J_c}] - K_{min}$ model). Note, larger values of m_σ would not be reliable, since in this case only very high stresses in a very small region near the crack tip would be sampled in the σ_w integration.

Figs. 15–17 show the results of application of these three models along with the pure $B^{-1/4}$ ($K_{min} = 0$) scaling model for comparison. The variation average $\langle K_{J_r} \rangle$ for all $b - B$ combinations as a function of B is shown in Fig. 15. The solid line is the least square fit to the data. The B dependence is negligible for the $m_\sigma = 15$ and 17 cases and larger in others, especially for the pure $B^{-1/4}$ ($K_{min} = 0$) scaling. Fig. 18 shows that the CDF for specimens with the three largest b are in good agreement, except for $m_\sigma = 19$. But, the K_{J_r} for specimens with the smallest $b = 3.2$ mm fall below the others in all cases, with the deviation increasing with decreasing m_σ. The corresponding CDF of $\langle K_{J_r} \rangle$ for all $b - B$ combinations shown in Fig. 17 have discontinuities at low to intermediate toughness for $m_\sigma = 15$ and, especially, $m_\sigma = 17$.

Following Gao and co-workers [17,18], $\sigma_{min} = 850$ MPa was determined for the $B = 25.4$ mm SSY σ_w value corresponding to a J_c at $K_{min} = 20$ MPa $\sqrt{m}$. The σ_u for various models defined by $P_f = 0.63$ are shown in Table 2. Fig. 18 shows the corresponding Weibull plots for K_{J_r}. All the models produce reasonable Weibull slopes ranging from $m_k = 3.65$ to 4.14 but the results for the B_{max} and p fits using the J_{crs} from the M_{lim} analysis AP is closest to the nominal value with $m_k = 3.94 \approx 4$. Fig. 19 shows the corresponding K_{J_r} predicted by the various $\sigma_w - [K_{J_m}/K_{J_c}] - K_{min}$ AP versus the optimized $\sigma^* - [K_{J_m}/K_{J_c}] - K_{min}$ AP. The constraint loss adjustments are larger for lower m_σ. As noted above, the overall discrepancy between the $\sigma_w - [K_{J_m}/K_{J_c}] - K_{min}$ versus $\sigma^* - [K_{J_m}/K_{J_c}] - K_{min}$ adjusted K_{J_r} is smallest at $m_\sigma = 17$, although on average the Weibull based K_{J_r} are generally still slightly lower (that is, the constraint loss adjustments are larger).

Based on all these considerations, it appears that the evaluation fitted p and B_{max} model with J_{crs} from the M_{lim} analysis, with $m_\sigma = 17$, provides the optimal procedure for a Weibull-based size AP. However, it also

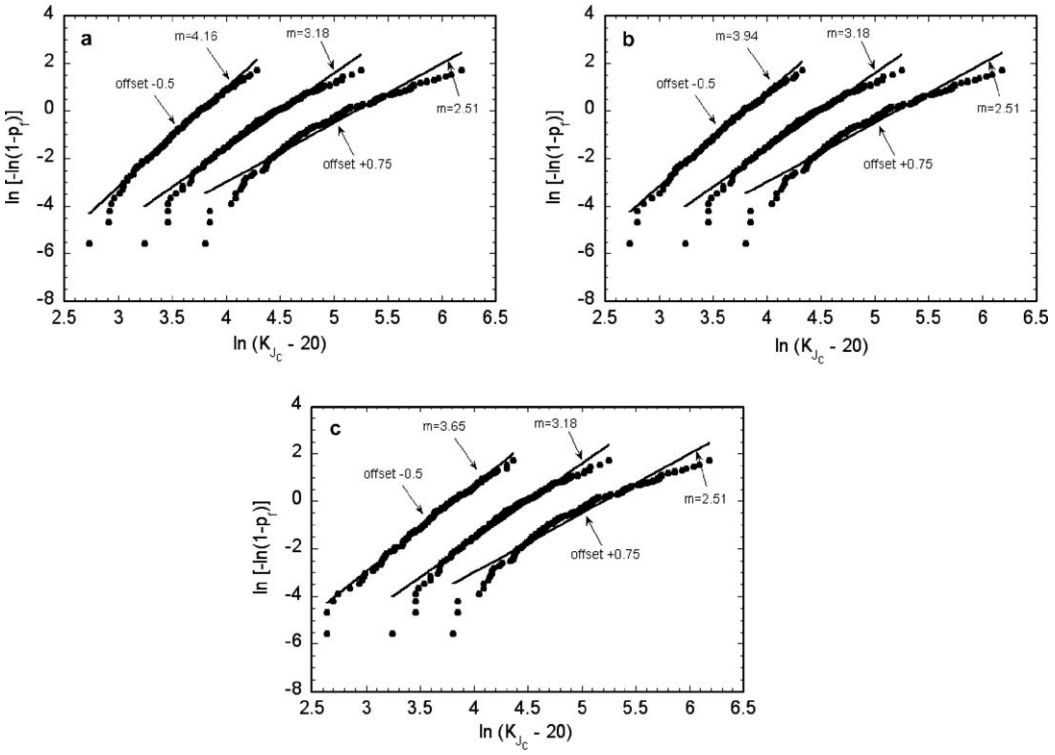

Fig. 18. Weibull plots of K_{J_c}, K_{J_B}, and $K_{J_m}\,\sigma_w - [K_{J_m}/K_{J_c}] - K_{min}$ AP with p and B_{max} fitted B-scaling model and: (a) $m_\sigma = 15$, (b) $m_\sigma = 17$ and (c) $m_\sigma = 19$.

Table 2
Fitted σ_u values for the three σ_w models

Model	σ_u (MPa)
$m_\sigma = 15$	1335
$m_\sigma = 17$	1385
$m_\sigma = 19$	1436

appears that the $\sigma^* - [K_{J_m}/K_{J_c}] - K_{min}$ AP is generally more reliable and easier to apply than any of the Weibull models, assuming calibration of the $R = \sigma^*/\sigma_y$ is possible.

4. Application of the $\sigma^* - [K_{J_m}/K_{J_c}] - K_{min}$ model to other data

The optimized $\sigma^* - [K_{J_m}/K_{J_c}] - K_{min}$ AP was also applied to the calibration data as well as other low constraint data measured in this study. The low constraint data was associated with either small specimen size or a shallow pre-crack. The former included $27 \times 5 \times 5$ mm and $18 \times 3.3 \times 3.3$ mm 3PB specimens with $a/W \approx 0.5$ scaled from the dimensions of a standard pre-cracked Charpy (PCC) designated as 1/2-PCCs and 1/3-PCCs. Shallow pre-cracked Charpy sized $55 \times 8 \times 10$ mm 3PB specimens with $a/W \approx 0.2$ were designated as SPCCs. The PCCs tested at −76 °C were also classified as low constraint specimens. All these specimens were side-grooved by $0.1B$ on both sides. Except for the temperature, the test procedures were generally similar to those described for the $b - B$ test matrix [6]. The $\sigma^* - [K_{J_m}/K_{J_c}] - K_{min}$ model was also applied to a large database of $243 K_{J_m}$ measurements on the Shoreham plate developed by Joyce and Tregoning for standard CT and 3PB specimen geometries with a range of sizes and tested over a range of temperatures [19–23].

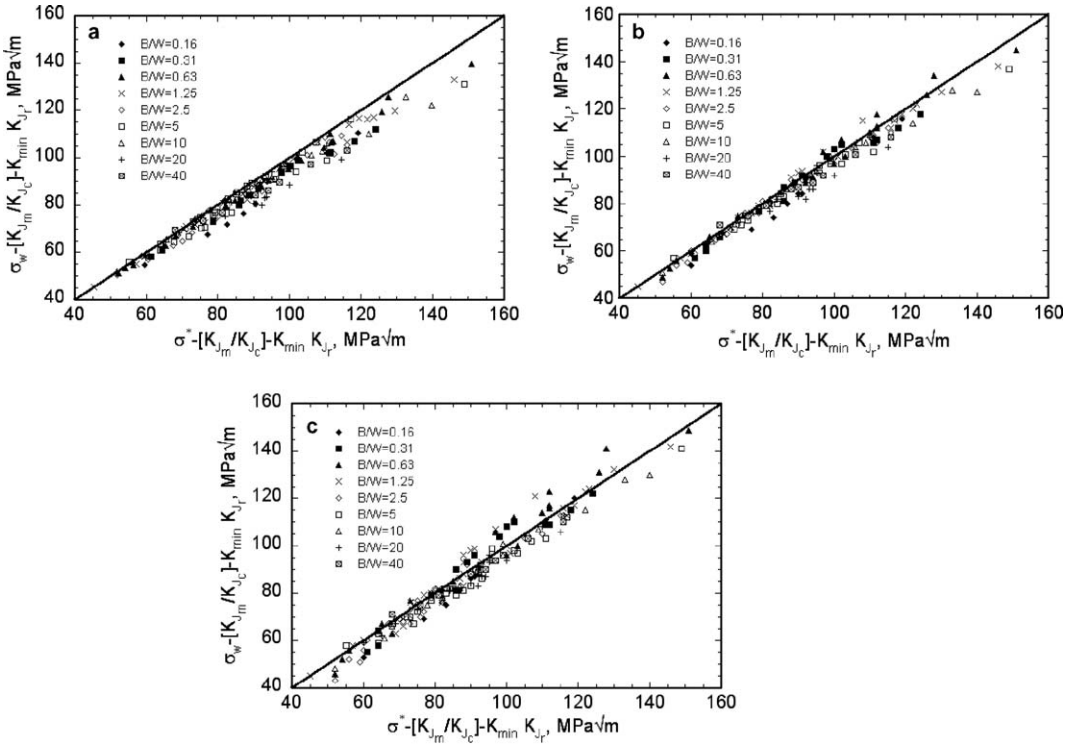

Fig. 19. Comparison the $\sigma_w - [K_{J_m}/K_{J_c}] - K_{min}$ versus $\sigma^* - [K_{J_m}/K_{J_c}] - K_{min}$ adjusted K_{J_r} for the p and B_{max} fitted B-scaling model and: (a) $m_\sigma = 15$, (b) $m_\sigma = 17$ and (c) $m_\sigma = 19$.

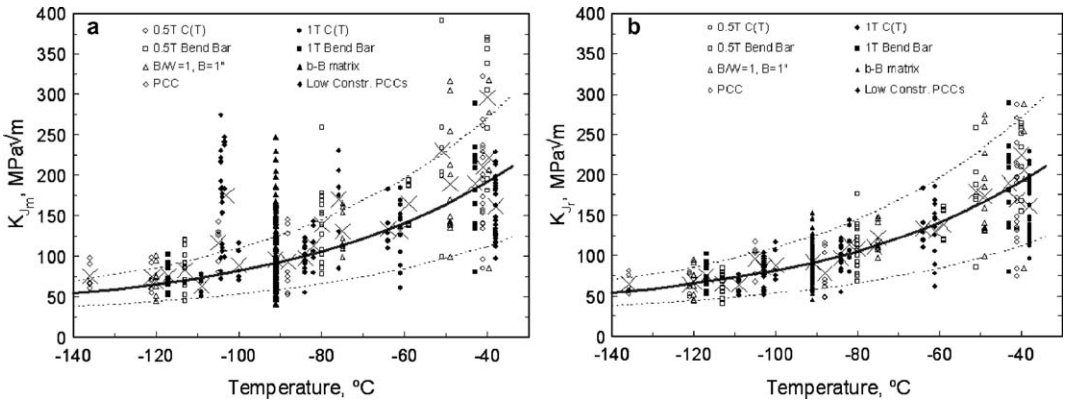

Fig. 20. The (a) measured K_{J_m} and (b) $\sigma^* - [K_{J_m}/K_{J_c}] - K_{min}$ adjusted K_{J_r} for the p and B_{max} fitted B-scaling model versus temperature for all the data measured in this study and the Joyce–Tregoning database and a master curve for $T_0 = -84$ °C.

Fig. 20 compares the measured K_{J_m} (Fig. 20a) and the size adjusted K_{J_r} (Fig. 20b) data for the entire Shoreham database consisting of 489 data points. This combined database covers an enormous and, indeed, unprecedented, range of specimen sizes and geometries. The solid and dashed lines in Fig. 20b are the median and 5% and 95% confidence intervals, respectively, with a $T_0 = -84$ °C found for the $b - B$ database based on the fitted p and B_{max} model. Clearly, the $\sigma^* - [K_{J_m}/K_{J_c}] - K_{min}$ AP is very effective in producing a size and geometry independent population of K_{J_r} data over a wide range of specimen configurations and test temperatures. Further, the K_{J_r} data are consistent with a single master curve with a T_0 of -84 °C.

5. Summary and conclusions

A large single variable database on effects of large variations in thickness (B) and ligament length (b) of 3PB specimens, described in a companion paper, was analyzed with a physically-based model treating both statistical and constraint loss mediated size effects. Our objectives were to: (1) decouple statistical (B) and constraint loss (b and B) size effects, and evaluate their interactions; (2) assess the validity and limits of theoretical $K_{\min}$ modified $B^{-1/4}$ statistical scaling arising from the K_J^4 scaling of the highly stressed process zone volume; (3) quantify the deformation (M) limits for approaching full constraint and the magnitude of the measured toughness (K_{J_m}) deviations beyond this limit versus small scale yielding (K_{J_c}); and (4) develop optimized procedures to adjust K_{J_m} to K_{J_c} and K_{J_c} to K_{J_r}. All of these objectives were met and led to the following conclusions:

- Both statistical and constraint loss effects occur over a wide range of specimen configurations and loading levels (see Fig. 11).
- The interaction between statistical and constraint loss effects is primarily due to reductions in K_{J_m} associated with large B that led to lower M, hence, higher constraint.
- However, the previous conclusion is modified for low B/b ratios due to rapid loss of out of plane constraint in geometrically thin specimens (see Fig. 4).
- The B-scaling of the adjusted K_{J_c} data is close to, but slightly less than the nominal value of $p = 1/4$ based on a assumed $K_{\min} = 20$ MPa $\sqrt{\text{m}}$. The $K_{\min}$ and p are strongly covariant. Higher $K_{\min}$ require a larger p and vice versa.
- Analysis of the $b - B$ database suggests that there may be an upper limit in the range of $B_{\max} \approx 150$ mm for statistical size scaling. However, this conclusion is tentative, and may be due to subtle experimental factors, and any such limit may vary from material to material. Nevertheless, this observation is certainly an issue that merits further research.
- Constraint loss begins at M less than ≈200 for typical B/b ratios and is significant at $M < 100$ (see Fig. 11). The potential effect of this result on possible non-conservative bias in the T_0 evaluated using the current ASTM E 1921 standard is discussed elsewhere [6].
- Two types of physical model-based procedures were successfully developed to adjust measured K_{J_m} to SSY K_{J_c} and K_{J_c} to a reference K_{J_r} at a reference B_r. The first method, based on an independently calibrated (σ^*) deterministic $\sigma^* - [K_{J_m}/K_{J_c}] - K_{\min}$ AP, was used to successfully decouple statistical and constraint loss mediated size effects in the $b - B$ database and to adjust this data to a single homogeneous population of K_{J_r} data well described by a single $T_0 = -84$ °C. While the $\sigma^* - [K_{J_m}/K_{J_c}] - K_{\min}$ AP may slightly over-adjust the data at the smallest $b = 3.2$ mm at higher toughness levels within this sub-population, a detailed evaluation of potential confounding factors and overall data trends suggests that this is probably not the case. The $\sigma^* - [K_{J_m}/K_{J_c}] - K_{\min}$ AP was optimized to account for both a $B_{\max}$ and a $p \approx 0.22$, slightly lower than the nominal value of 0.25. However, B-scaling based on the ASTM E 1921 procedure also worked fairly well.
- The $\sigma^* - [K_{J_m}/K_{J_c}] - K_{\min}$ procedure was also used to adjust other UCSB high and low constraint data as well as a large independent database on the Shoreham steel taken from the literature for tests on conventional 3PB and CT specimens tested over a range of temperatures. The overall adjusted database composed of 489K_{J_r} values was also well-represented by a MC with $T_0 \approx -84$ °C.
- Self-calibrated statistical Weibull-type, $\sigma_w - [K_{J_m}/K_{J_c}] - K_{\min}$, models were also reasonably successful in adjusting the K_{J_m} to a homogeneous population of size independent K_{J_r} data. However, there is not a single best or unique method to self-calibrate the model for an optimized value of the Weibull modulus, m_σ, which ranged from about 12 to 20, depending on details of the self-calibration method and choice of the B-scaling model. The most successful calibration, which minimized the overall size and geometry effects in the K_{J_r} database, was based on assessing small scale yielding values of J_{crs} from a $M_{\lim}$ analysis. This analysis evaluated the K_{J_0} using the E 1921 procedure, but with an adjustable M censoring limit ($M_{\lim}$) that increased over the value of 30 in the E 1921 Standard, up to the level where K_{J_0} becomes independent of $M_{\lim}$ (≈200). Coupled with the best-fit values of $B_{\max}$ and p found in the analysis using the $\sigma^* - [K_{J_m}/K_{J_c}] - K_{\min}$ AP suggests an optimal $m_\sigma \approx 17$. The optimized $m_\sigma = 17$, $\sigma_w - [K_{J_m}/K_{J_c}] - K_{\min}$ AP slightly over-adjusts the K_{J_m} data relative to the $\sigma^* - [K_{J_m}/K_{J_c}] - K_{\min}$ AP.

- The apparent over-adjustments of the $\sigma_w - [K_{J_m}/K_{J_c}] - K_{min}$ procedure increased with decreasing m_σ. This is a result of the increased weighting given to lower crack tip principal stress, σ_1, values with larger constraint loss effects in deeply cracked bend geometries. Higher values of m_σ suffer both computational limits and become physically suspect due to the small values of the volume which contribute to σ_w. More generally, the $\sigma_w - [K_{J_m}/K_{J_c}] - K_{min}$ AP was not as effective in eliminating size effects and was more difficult to implement compared to the $\sigma^* - [K_{J_m}/K_{J_c}] - K_{min}$ AP.
- The use of a calibrated $\sigma^* - [K_{J_m}/K_{J_c}] - K_{min}$ model to adjust K_{J_m} data to K_{J_r} is a very attractive possibility and has been successfully applied to evaluating T_0 for a 8Cr martensitic steel [24]. The major limitation is having sufficient high constraint data to calibrate a reliable value of $R = \sigma^*/\sigma_y$. However, in principle it is possible to estimate σ^* based on corresponding estimates of T_0 and practical approaches to using this method where high constraint data are more limited are under development.

Finally, other outstanding interrelated questions not resolved, or even addressed, in this work include: (1) the possible existence of a minimum B for statistical size scaling; (2) the overall question of a physically minimum value lower bound toughness; (3) the basis for a K_{min} and its potential alloy to alloy variation and dependence on temperature/toughness level; (4) the validity of Weibull statistics for the lower and upper tails in toughness distributions; (5) the existence of, physical basis for and fracture mechanism limits on a universal toughness–temperature curve shape; (6) the effects of irradiation, and other in-service degradation mechanisms, on the validity of various assumptions and procedures used in the master curve method. All of these issues are the subject of ongoing research and it is noted that the extremely detailed and comprehensive database on the Shoreham steel makes it an ideal candidate for use in such studies.

Acknowledgements

This work was primarily funded by US Nuclear Regulatory Commission (NRC) Contracts NRC-04-94-049 and NRC-04-01-064. We give special thanks to Robert Tregoning, previously at the Carderock Division Naval Surface Warfare Center, and more recently at the US NRC. Rob's helpful advice and insightful comments, as well as his generous assistance in the both the testing we did at Carderock and in providing his outstanding database, were key elements in completing this work. The encouragement and support of our NRC project monitors, the late Mike Vassilaros, who helped us to initiate this project, and more recently Carolyn Fairbanks and Tanny Santos, were critical to our effort. The authors also gratefully acknowledge Joe Waskey at Carderock and Tom Huang at UCSB for their assistance in testing and data evaluation. The authors also acknowledge Professor Robert Dodds and Jason Petti of the University of Illinois for their advice on application of the Weibull stress model. The always generous support and numerous helpful suggestions of many members of the UCSB Materials Performance and Reliability Group are also much appreciated.

References

[1] Dodds Jr RH, Anderson TL, Kirk MT. A framework to correlate a/W ratio effects on elastic–plastic fracture toughness (J_c). Int J Fract 1991;48:1–22.
[2] Anderson TL. Fracture mechanics: fundamentals and applications. 3rd ed. Boca Raton, Florida: CRC Press; 2005.
[3] Petti JP, Dodds Jr RH. Constraint comparisons for common fracture specimens: $C(T)$s and SE(B)s. Engng Fract Mech 2004;71:2677–83.
[4] ASTM E 1921-97. Standard test method for determination of reference temperature, T_0, for ferritic steels in the transition range. ASTM, 2004.
[5] Merkle JG, Wallin K, McCabe DE. Technical basis for an ASTM standard on determining the reference temperature, T_0, for ferritic steels in the transition range. NUREG/CR-5504, ORNL/TM-13631, 1998.
[6] Rathbun HJ, Odette GR, Yamamoto T, He MY, Lucas GE. Statistical and constraint loss size effects on cleavage fracture – implications to measuring toughness in the transition. J Press Ves Technol, in press.
[7] Rathbun HJ, Odette GR, Yamamoto T, Lucas GE. Influence of statistical and constraint loss size effects on cleavage fracture toughness in the transition – a single variable experiment and database. Engng Fract Mech 2006;73:134–58.
[8] Rathbun HJ, Odette GR, He MY, Lucas GE, Sheckherd JW. Statistical versus constraint size effects on the transition regime toughness: a preliminary study of a pressure vessel steel. Fracture, fatigue and weld residual stress, PVP-vol. 393. American Society of Mechanical Engineers; 1999. p. 17–22.

[9] Evans AG. Statistical aspects of cleavage fracture in steel. Metall Trans A 1983;14A:1349–55.
[10] Odette GR. On the ductile to brittle transition in martensitic stainless steels: mechanisms, models, and structural implications. J Nucl Mater 1994;212–215:45–51.
[11] Williams TJ, Swan DI, Dixon GL. Modification of the tail of the master curve distribution. In: Proceedings of the IAEA technical meeting on irradiation effects and mitigation in reactor pressure vessel steels, Gus Khrustalny, Russia, May 24–28, 2004.
[12] Hibbit, Karlsson and Sorenssen, Inc., ABAQUS Users Manual 5.8, 1998.
[13] Nevalainen M, Dodds Jr RH. Numerical investigation of 3-D constraint effects on brittle fracture in $SE(B)$ and $C(T)$ specimens. Int J Fract 1995;74:131–61.
[14] Odette GR, He MY. A cleavage toughness master curve model. J Nucl Mater 2000;283–287:120–7.
[15] Rathbun HJ, Odette GR, He MY, Lucas GE, Yamamoto T. Size scaling of cleavage toughness in the transition: a single variable experiment and model-based analysis. NUREG/CR-6790, in press.
[16] Beremin FM. A local criterion for cleavage fracture of a nuclear pressure vessel steel. Metall Trans A 1983;14A:2277–87.
[17] Gao XS, Ruggieri C, Dodds Jr RH. Calibration of Weibull stress parameters using fracture toughness data. Int J Fract 1998;92:175–200.
[18] Gao XS, Dodds Jr RH. An engineering approach to assess constraint effects on cleavage fracture toughness. Engng Fract Mech 2001;68(3):263–83.
[19] Tregoning RL, Joyce JA. T_0 evaluation in common specimen geometries. Applications of fracture mechanics in failure assessment, PVP-vol. 412. ASME; 2000.
[20] Joyce JA, Tregoning RL. Effects of materials inhomogeneity on the T_0 reference temperature in thick section A533B plate. In: ASME Pressure vessels and piping conference proceedings, 2001.
[21] Tregoning RL, Joyce JA. Application of a T-stress based constraint correction to A533B steel fracture toughness data. ASTM Special Technical Publication, no. 1417. 2002. p. 307–27.
[22] Joyce JA, Tregoning RL. Development of the T_0 reference temperature from precracked Charpy specimens. Engng Fract Mech 2001;68(7):861–94.
[23] Tregoning RL, Joyce JA. Investigation of censoring limits for cleavage fracture determination. In: Sokolov MA, Landes JD, Lucas GE, editors. Small specimen test techniques, vol. 4, ASTM STP 1418. West Conshocken, PA: ASTM; 2001.
[24] Odette GR, Yamamoto T, Kishimoto H, Sokolov M, Spatig P, Yang WJ, et al. A master curve analysis of F82H using statistical and constraint loss size adjustments of small specimen data. J Nucl Mater 2004;329–333:1243–7.